MINISTRY OF EDUCATION AND SCIENCE OF UKRAINE
NATIONAL AVIATION UNIVERSITY
Department of aircraft design

APPROVED BY
Head of department
Professor, Dr. of Sc.
_____S.R. Ignatovych
«___» _____ 2020.

MASTER THESIS
(EXPLANATORY NOTE)

GRADUATE OF EDUCATIONAL DEGREE
«MASTER»

ACCORDING TO THE EDUCATIONAL PROFESSIONAL PROGRAM
«AIRCRAFT EQUIPMENT »

Theme: « Application of Fractal geometry to the fatigue analysis of aluminum structures »

Prepared by: **_____V.V. Bondar**

Supervisor: PhD, associate professor **_____T.P. Maslak**

Consultants on individual sections of the explanatory note:
labor protection: Ph.d., associate professor **_____O.V. Konovalova**
environmental protection:
Ph.d., associate professor **_____L.I. Pavliukh**

Normocontroller **_____ S.V. Khiznyak**

Kyiv 2020

NATIONAL AVIATION UNIVERSITY

Faculty aerospace
Department of aircraft design
Educational degree «Master»
Specialty 134 «Aviation and space rocket technology»
Educational professional program «Aircraft equipment»

APPROVED BY
Head of department
Dr. Sc., professor
_____S.R. Ignatovych
«___» _____ 2020.

TASK

for the master thesis

VALERII BONDAR

1. Topic: «Application of Fractal geometry to the fatigue analysis of aluminum structures», approved by Rector's order № 1906/ст_ from 5 october 2020 year.
2. Period of work execution: from 5 October 2020 year to 13 December 2020 year.
3.Initial data theories of multiaxial loading estimations, material specimens made from D16AT, four modes of loading and equivalent stress equal to 150 MPa.
4.Content (list of topics to be developed): multiaxial loading of aircraft structural components,structural components of the aircraft subjected to the multiaxial loading, experimental methods for the multiaxial stress-strain state analyses; materials, equipment and procedures; specimens, equipment for the fatigue tests under multiaxial loading; experimental test, analytical test simulation; method for the multiaxial fatigue damage assessment of aircraft components; finite element analyses of the stress-strain state of the specimens for different modes of loading; deformation relief as an indicator of multiaxial fatigue damage.
5. Required material: placards illustrating the results of surface relief damage accumulation after four different regimes of loading (A2×6).

Microsoft Office Excel, CATIA, Abaqus, light and scan microscopy should be used to provide graphic support materials.

6. Thesis schedule

№	Task	Execution period	Done
1	Investigation of structural components of the aircraft subjected to the multiaxial loading.	5.10.2020–6.10.2020	
2	Researching of experimental methods for the multiaxial stress-strain state analyses.	7.10.2020–15.10.2020	
3	Conducting the multiaxial fatigue stress experimental test.	16.10.2020–20.10.2020	
4	Analytical investigation of the multiaxial fatigue damage and CAE test simulation.	21.10.2020–30.10.2020	
5	Execution of the parts, devoted to environmental and labour protection.	30.10.2020–10.11.2020	
6	Preparation of illustrative material, writing the report.	11.11.2020–24.11.2020	
7	Explanatory note checking, editing and correction.	25.11.2020–05.12.2020	

7. Special chapter consultants

Chapter	Consultant	Date, signature	
		Task Issued	Task Received
Labor protection	Ph.d., associate professor O.V. Konovalova		
Environmental protection	Ph.d., associate professor L.I. Pavliukh		

8. Date of issue of the task: «___»_____2020 year.

Thesis supervisor _____ T.P. Maslak

Task accepted for execution _____V.V. Bondar

ABSTRACT

Explanatory note to the master's thesis «Application of Fractal geometry to the fatigue analysis of aluminum structures» contains:

99 sheets, 53 figures, 14 tables, 47 references

The object of study - the process of accumulation of fatigue damage in the weeping layer of aluminum alloy D16AT.

The subject of research is the evolution of quantitative parameters of the deformation relief of the cladding layer of structural aluminum alloy under cyclic loading.

Research methods: fatigue testing of samples of structural materials; optical microscopy methods; automated calculation of deformation relief parameters based on its digital images; methods of fractal geometry.

Scientific novelty of the obtained results:

1. Have used fractal dimension as a quantitative indicator of fatigue damage to the fuselage skin.

2. It is proved that the deformation relief, which is formed on the surface of the cladding layer of aluminum alloy D16AT as a result of cyclic loading, is an irregular stochastic fractal. To assess the accumulated fatigue damage, it is advisable to use the fractal dimension, which is determined from the ratio of the perimeter of the clusters of deformation relief to their area.

3. It is shown that the selected parameters of the deformation relief change monotonically under cyclic loading, are sensitive to the level of the maximum stress of the loading cycle.

4. The evolution of quantitative parameters of deformation relief in the process of loading is obtained, which allow to take into account the influence of loading modes on the process of accumulation of fatigue damage of D16AT alloy.

The practical significance of the results obtained is that:

1. the presented parameter of the deformation relief can be used to assess the accumulated fatigue damage of structural aluminum alloys during field tests of the aircraft fuselage; during laboratory fatigue tests of elements of aircraft structures;

in the educational process in specialties that involve the study of problems of design and testing of aircraft.

KEYWORDS: AIRCRAFT, MULTIAXIAL LOADING, EQUIVALENT STRESS, LIGHT AND SCAN MICROSCOPY, MORPHOLOGY OF SURFACE RELIEF DAMAGE, PERSISTENT SLIP BAND, EXTRUSION, INTRUSION, FINITE ELEMENT METHOD, DAMAGE FACTOR.

CONTENTS

INTRODUCTION 13

1 FRACTAL GEOMETRY APPLICATION IN THE TASK OF MATERIAL SCIENCE 14

1.1 Fundamentals of fractal geometry 14

1.1.1 Mandelbrot set 17

1.1.2 Julia sets 19

1.1.3 Sierpinski Triangle 21

1.1.4 Koch Snowflake 22

1.2 Fractals applications 24

1.2.1 Fractals in astrophysics 24

1.2.2 Fractals in the Biological Sciences 24

1.2.3 Fractals in computer graphics 25

1.3 Fractal Dimension as a quantitive parameter of regular structures 26

CONCLUSION TO THE PART 1 30

2 METHODOLOGY OF THE DEFORMATION REIEF ESTIMATION BY THE FRACTAL DIMENSION 31

2.1 Introduction 31

2.2 Object of the investigation. Materials and specimens 31

2.3 Equipment for the investigation 35

2.4 Application of Finite Element Method for stress-strain analysis 38

2.5 The algorithm of the experiment 40

2.6 Images analysis 42

CONCLUSION ON THE PART 2 43

3 FRACTAL GEOMETRY APPLICATION FOR THE FATIGUE DAMAGE MONITORING OF D16AT STRUCTURAL ALLOY 44

3.1 Fractality of the deformation relief clusters 44
3.2 Selection of deformation relief parameters for assessment of accumulated damage and prediction of residual life 51
3.3 Influence of the level of maximum stress of the load cycle on the development of deformation relief 60
CONCLUSION OF THE PART 3 65

4 LABOUR PROTECTION 66
4.1 Analysis of harmful and dangerous production factors 66
4.1.1 Working conditions analysis 66
4.1.2 List of harmful and dangerous factors 69
4.2 Measures to reduce the impact of harmful and dangerous production factors……...69
4.2.1 Working out the measures for labour protection improvement 72
4.2.2 Fire safety 72
4.2.3 Artificial lighting calculation 74
4.3 Occupational Safety Instruction 75
4.3.1 General safety requirements 75
4.3.2 Safety Requirements before starting work 76
4.3.3 Safety Requirements during operation 79
4.3.4 Safety Requirements after work 81
4.3.5 Safety Requirements at emergency situations 82
CONCLUSION OF THE PART 3 84

5 ENVIRONMENTAL PROTECTION 85
5.1 Introduction 85
5.2 Environmental pollution classification 86
5.2.1 Acoustic pollution 86
5.2.2 Water pollution 87

5.2.3 Air quality. Particulate matter emissions 88
5.2.4 Chemical pollution 89
5.2.5 Radiation exposure 90
5.2.6 Changing of the climate 91
5.2.7 Aircraft Engine Emissions 92
5.3 Multiaxial stress test environmental conditions 94
CONCLUSION TO PART 5 97
GENERAL CONCLUSIONS 98
REFERENCES 99

INTRODUCTION

Fractals is a new branch of mathematics and art. Perhaps this is the reason why most people recognize fractals only as pretty pictures useful as backgrounds on the computer screen or original postcard patterns.

Most physical systems of nature and many human artifacts are not regular geometric shapes of the standard geometry derived from Euclid. Fractal geometry offers almost unlimited ways of describing, measuring and predicting these natural phenomena. But is it possible to define the whole world using mathematical equations.

This article describes how the four most famous fractals were created and explains the most important fractal properties, which make fractals useful for different domain of science.

Analysis of the literature indicates the emergence of studies that effectively use the apparatus of fractal geometry. The range of problems of fractal geometry is quite wide. Consider the basic concepts of fractal geometry. Thus, a fractal is a structure consisting of parts that are in some sense similar to the whole and have a fractal dimension; fractality - the property of an object to be a fractal or a dimension to be fractal; fractal dimension is a dimension that cannot necessarily take integer values.

Many people are fascinated by the beautiful images termed fractals. Extending beyond the typical perception of mathematics as a body of complicated, boring formulas, fractal geometry mixes art with mathematics to demonstrate that equations are more than just a collection of numbers. What makes fractals even more interesting is that they are the best existing mathematical descriptions of many natural forms, such as coastlines, mountains or parts of living organisms.

1 FRACTAL GEOMETRY APPLICATION IN THE TASK OF MATERIAL SCIENCE

In construction materials production the application of the theory of fractal geometry allows revealing a new possibility to model the properties of materials and processes. The fractal theory can be used in the research of the processes of cement paste hardening as the formation of a cluster structure; cracking caused by various factors, using data received at predicting the collapse of critical structures; the structure and properties of dispersed media; structural characteristics of the porous material. The investigation of surface properties of aggregate, using a fractal approach, allowed one to reveal the direct dependence between the physical and mechanical characteristics of the concrete and the value of the fractal dimension of such aggregate. Thus, application of the method based on the determination of the fractal dimension of the aggregate, allows predicting the properties of concrete as well as to regulate its physical and mechanical properties by selecting or modifying the composition of the aggregate grain size, using the estimation of its fractal dimension.

1.1 Fundamentals of fractal geometry

Fractal geometry is closely connected with computer techniques, some people had worked on fractals long before the invention of computers. Those people [1 *Weisstein, Eric W.* Coastline Paradox Wolfram MathWorld, 2 Ashford, Oliver M., Charnock, H., Drazin, P. G., Hunt, J. C. R. The Collected Papers of Lewis Fry Richardson / Ed. Ashford, Oliver M. — Cambridge University Press, 1993. — P. 45-46. — (Vol. 1. Meteorology and numerical analysis).] were British cartographers, who encountered the problem in measuring the length of Britain coast. The coastline measured on a large scale (Figure - 1.1 a) map was approximately half the length of coastline measured on a detailed map (fig 1.1 b).

The closer they looked, the more detailed and longer the coastline became. They did not realize that they had discovered one of the main properties of fractals –

fractal dimension. In the Figure - 1.1 we can see the example of a Coastline paradox by Lewis Richardson

a) b)

Figure 1.1 - Coastline paradox by Lewis Fry Richardson: a) - geodesic interval in 100 km, length of coastline is 2800 km, b) - geodesic interval in 50 km, length of coastline is 3400 km

Two of the most important properties of fractals are self-similarity and non-integer dimension.

What does self-similarity mean? If you look carefully at a fern leaf, you will notice that every little leaf part of the bigger one has the same shape as the whole fern leaf. You can say that the fern leaf is self-similar. The same is with fractals: you can magnify them many times and after every step you will see the same shape, which is characteristic of that particular fractal.

The non-integer dimension is more difficult to explain. Classical geometry deals with objects of integer dimensions: zero dimensional points, one dimensional lines and curves, two dimensional plane Figure -s such as squares and circles, and three dimensional solids such as cubes and spheres. However, many natural phenomena are better described using a dimension between two whole numbers.

While a straight line has a dimension of one, a fractal curve will have a dimension between one and two, depending on how much space it takes up as it twists and curves. The more the flat fractal fills a plane, the closer it approaches two dimensions. Likewise, a "hilly fractal scene" will reach a dimension somewhere between two and three. A fractal landscape made up of a large hill covered with tiny mounds would be close to the second dimension, while a rough surface composed of many medium-sized hills would be close to the third dimension.

The basic concepts of fractal geometry is a structure consisting of parts (clusters), which at that time understands the similar whole and has a fractal dimension; fractality - the property of an object to be fractal or size to be fractal; fractal dimension is a dimension that cannot necessarily take integer values.

There are a lot of different types of fractals, two of the most popular types: complex number fractals and Iterated Function System (IFS) fractals.

A complex number consists of a real number added to an imaginary number. It is common to refer to a complex number as a "point" on the complex plane. If the complex number is:

$$z = (a + b \cdot i) \tag{1.1}$$

the coordinates of the point are: a (horizontal - real axis) and b (vertical – imaginary axis).

The unit of imaginary numbers:

$$i = \sqrt{(-L)} \tag{1.2}$$

Two leading researchers in the field of complex number fractals are Gaston Maurice Julia and Benoit Mandelbrot. Gaston Maurice Julia was born at the end of 19th century in Algeria. He spent his life studying the iteration of polynomials and rational functions. Around the 1920s, after publishing his paper on the iteration of a rational function, Julia became famous. However, after his death, he was forgotten. In the 1970s, the work of Gaston Maurice Julia was revived and popularized by the Polish-born Benoit Mandelbrot. Inspired by Julia’s work.

With the help of computer graphics, IBM employee Mandelbrot was able to show the first pictures of the most beautiful fractals known today.

1.1.1 Mandelbrot set

The Mandelbrot set is the set of points on a complex plain. To build the Mandelbrot set, we have to use an algorithm based on the recursive formula:

$$Z_n = Z_{n-1}^2 + C \tag{1.3}$$

separating the points of the complex plane into two categories:

- points inside the Mandelbrot set,
- points outside the Mandelbrot set.

The image (Figure -1.2) below shows a portion of the complex plane

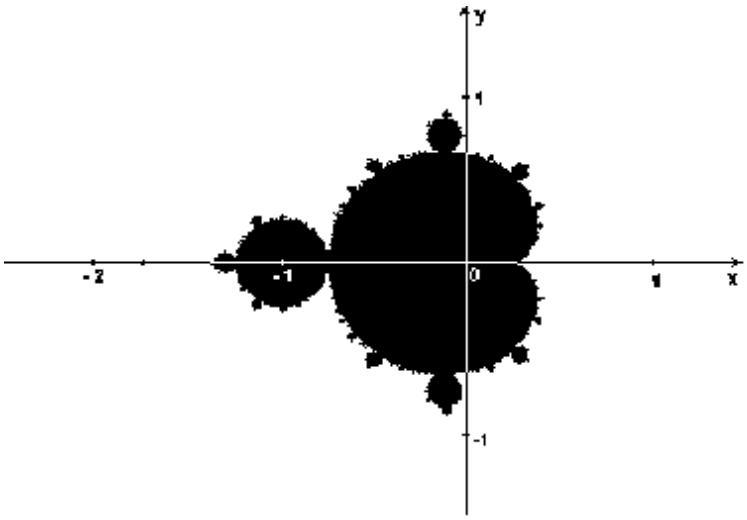

Figure 1.2 - The points of the Mandelbrot set have been colored black.

It is also possible to assign a color to the points outside the Mandelbrot set (Figure -1.3). Their colors depend on how many iterations have been required to determine that they are outside the Mandelbrot set.

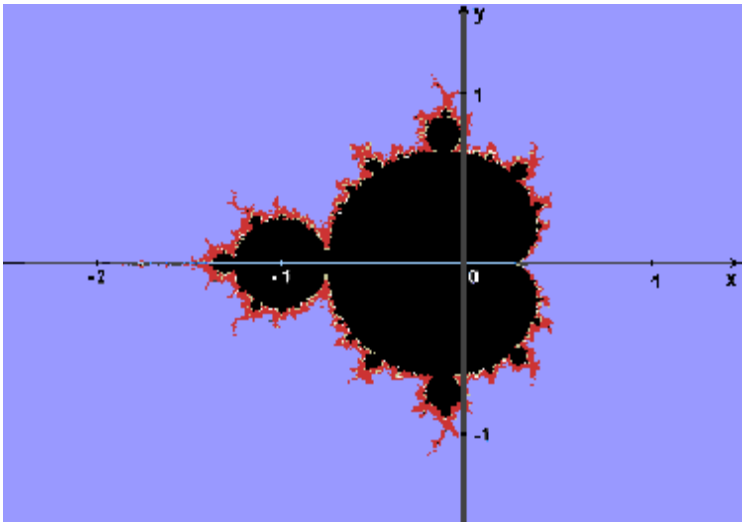

Figure 1.3 - Mandelbrot set

To create the Mandelbrot set we have to pick a point (*C*) on the complex plane. The complex number corresponding with this point has the form:

$$c = a + b \cdot i \tag{1.4}$$

After calculating the value of previous expression:

$$z = z_0^2 + C \tag{1.5}$$

Using zero as the value of z_0, we obtain *C* as the result. The next step consists of assigning the result to z_1 and repeating the calculation: now the result is the complex number C_2+C . Then we have to assign the value to and repeat the process again and again.

This process can be represented as the "migration" of the initial point *C* across the plane. What happens to the point when we repeatedly iterate the function? Will it remain near to the origin or will it go away from it, increasing its distance from the origin without limit? In the first case, we say that *C* belongs to the Mandelbrot set (it is one of the black points in the image); otherwise, we say that it goes to infinity and

we assign a color to *C* depending on the speed at which the point "escapes" from the origin.

We can take a look at the algorithm from a different point of view. Let us imagine that all the points on the plane are attracted by both: infinity and the Mandelbrot set. That makes it easy to understand why:

- points far from the Mandelbrot set rapidly move towards infinity,
- points close to the Mandelbrot set slowly escape to infinity,
- points inside the Mandelbrot set never escape to infinity.

1.1.2 Julia sets

Julia sets are strictly connected with the Mandelbrot set. The iterative function that is used to produce them is the same as for the Mandelbrot set. The only difference is the way this formula is used. In order to draw a picture of the Mandelbrot set, we iterate the formula for each point *C* of the complex plane, always starting with $z_0 = 0$. If we want to make a picture of a Julia set, *C* must be constant during the whole generation process, while the value of varies. The value of *C* determines the shape of the Julia set; in other words, each point of the complex plane is associated with a particular Julia set.

We have to pick a point *C*) on the complex plane. The following algorithm determines whether or not a point on complex plane *Z*) belongs to the Julia set associated with *C*, and determines the color that should be assigned to it. To see if *Z* belongs to the set, we have to iterate the function

$$z_1 = z_0^2 + C \tag{1.6}$$

Using $z_0 = z$. What happens to the initial point Z when the formula is iterated? Will it remain near to the origin or will it go away from it, increasing its

distance from the origin without limit? In the first case, it belongs to the Julia set; otherwise it goes to infinity and we assign a color to Z depending on the speed the point "escapes" from the origin. To produce an image of the whole Julia set associated with C, we must repeat this process for all the points Z whose coordinates are included in this range:

$$-2 < a < 2\ ;\ -1.5 < y < 1.5$$

The most important relationship between Julia sets and Mandelbrot set is that while the Mandelbrot set is connected (it is a single piece), a Julia set is connected only if it is associated with a point inside the Mandelbrot set. For example: the Julia set associated with p C_1 is connected; the Julia set associated with C_1 is not connected (see picture below).

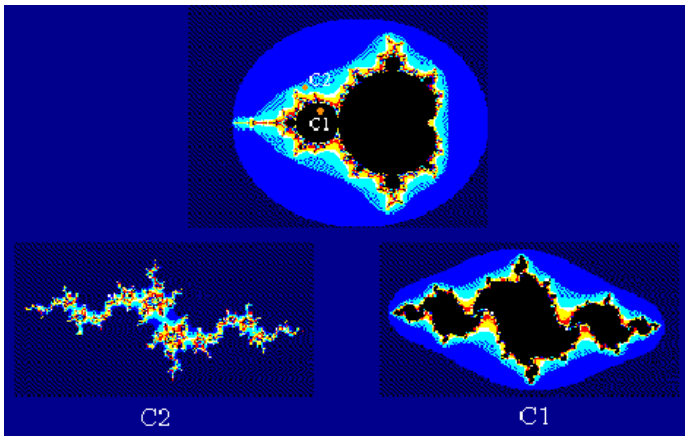

Figure 1.4 - A single piece between Mandelbrot set and Julia set

Iterated Function System Fractals

Iterated Function System (IFS) fractals are created on the basis of simple plane transformations: scaling, dislocation and the plane axes rotation. Creating an IFS fractal consists of following steps:

1. defining a set of plane transformations,
2. drawing an initial pattern on the plane (any pattern),

3. transforming the initial pattern using the transformations defined in first step,

4. transforming the new picture (combination of initial and transformed patterns) using the same set of transformations,

5. repeating the fourth step as many times as possible (in theory, this procedure can be repeated an infinite number of times).

The most famous ISF fractals are the Sierpinski Triangle and the Koch Snowflake.

1.1.3 Sierpinski Triangle

This is the fractal we can get by taking the midpoints of each side of an equilateral triangle and connecting them. The iterations should be repeated an infinite number of times. The pictures below present four initial steps of the construction of the Sierpinski Triangle:

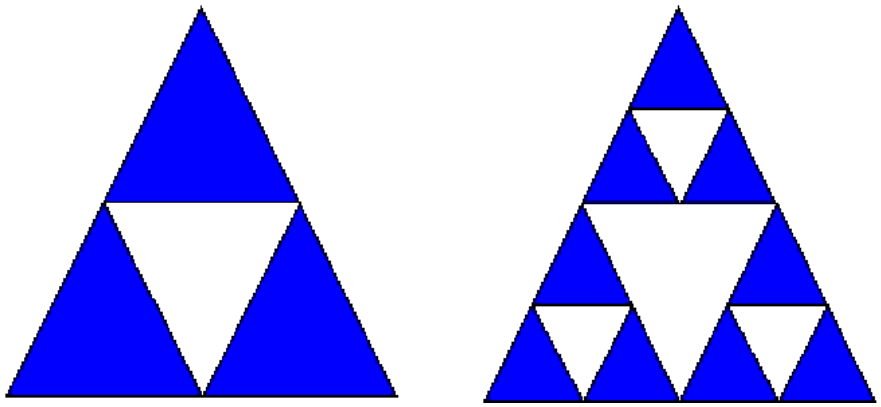

1) 2)

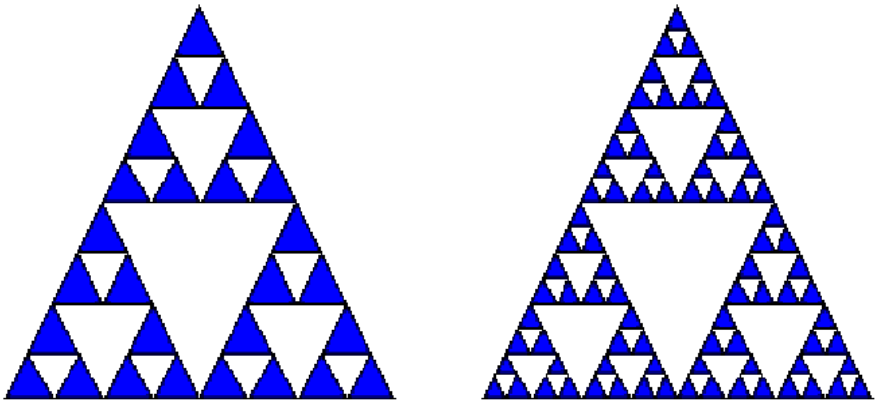

3) 4)

Figure 1.5 - Four initial steps of the construction of the Sierpinski Triangle

Using this fractal as an example, we can prove that the fractal dimension is not an integer.

First of all we have to find out how the "size" of an object behaves when its linear dimension increases. In one dimension we can consider a line segment. If the linear dimension of the line segment is doubled, then the length (characteristic size) of the line has doubled also. In two dimensions, if the linear dimensions of a square for example is doubled then the characteristic size, the area, increases by a factor of 4. In three dimensions, if the linear dimension of a box is doubled then the volume increases by a factor of 8.

This relationship between dimension D, linear scaling L and the result of size increasing S can be generalized and written as:

$$S = L \cdot D \tag{1.7}$$

Rearranging of this formula gives an expression for dimension depending on how the size changes as a function of linear scaling:

$$D = \frac{\log(s)}{\log(L)}$$

(1.8)

In the examples above the value of D is an integer - 1, 2, or 3 - depending on the dimension of the geometry. This relationship holds for all Euclidean shapes. How about fractals?

Looking at the picture of the first step in building the Sierpinski Triangle, we can notice that if the linear dimension of the basis triangle (L) is doubled, then the area of whole fractal (blue triangles) increases by a factor of three (S).

Using the pattern given above, we can calculate a dimension for the Sierpinski Triangle:

$$D = \frac{\log(3)}{\log(2)} = \mathbf{1.585} \tag{1.9}$$

The result of this calculation proves the non-integer fractal dimension.

1.1.4 Koch Snowflake

To construct the Koch Snowflake, we have to begin with an equilateral triangle with sides of length, for example, 1. In the middle of each side, we will add a new triangle one-third the size; and repeat this process for an infinite number of iterations. The length of the boundary is $3 \cdot \frac{4}{3} \cdot \frac{4}{3} \cdot \frac{4}{3} \ldots$ -infinity.

However, the area remains less than the area of a circle drawn around the original triangle. That means that an infinitely long line surrounds a finite area. The end construction of a Koch Snowflake resembles the coastline of a shore.

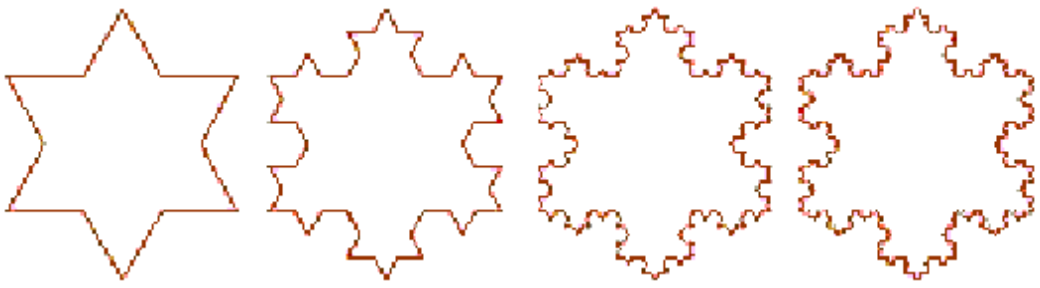

Figure 1.6 - Four steps of Koch Snowflake construction

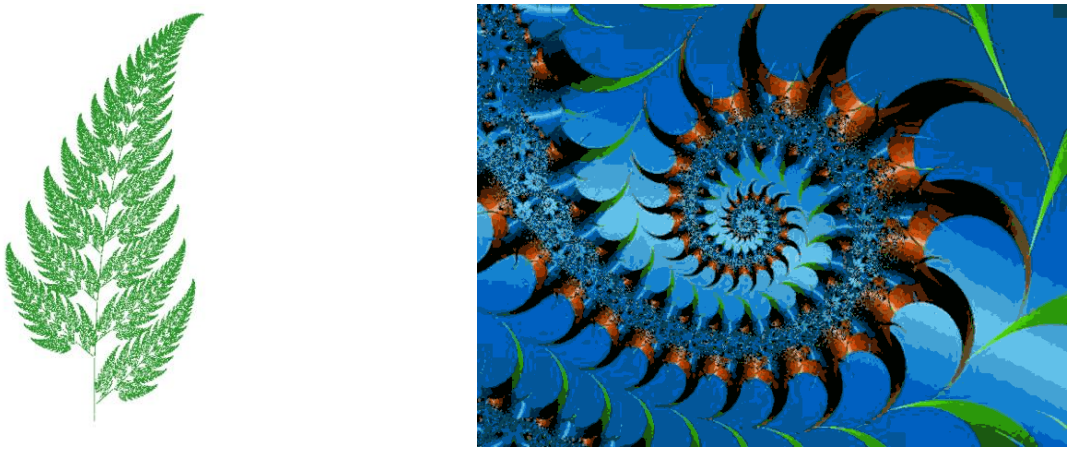

Fern leaf Spiral

Figure 1.7 - IFS fractals

1.2 Fractals applications

Fractal geometry has permeated many area of science, such as astrophysics, biological sciences, and has become one of the most important techniques in computer graphics.

1.2.1 Fractals in astrophysics

Nobody really knows how many stars actually glitter in our skies, but have you ever wondered how they were formed and ultimately found their home in the Universe. Astrophysicists believe that the key to this problem is the fractal nature of interstellar gas. Fractal distributions are hierarchical, like smoke trails or billowy clouds in the sky. Turbulence shapes both the clouds in the sky and the clouds in space, giving them an irregular but repetitive pattern that would be impossible to describe without the help of fractal geometry.

1.2.2 Fractals in the Biological Sciences

Biologists have traditionally modeled nature using Euclidean representations of natural objects or series. They represented heartbeats as sine waves, conifer trees as cones, animal habitats as simple areas, and cell membranes as curves or simple surfaces. However, scientists have come to recognize that many natural constructs are better characterized using fractal geometry. Biological systems and processes are typically characterized by many levels of substructure, with the same general pattern repeated in an ever-decreasing cascade.

Scientists discovered that the basic architecture of a chromosome is tree-like; every chromosome consists of many 'mini-chromosomes', and therefore can be treated as fractal. For a human chromosome, for example, a fractal dimension *D* equals *2,34* (between the plane and the space dimension).

Self-similarity has been found also in DNA sequences. In the opinion of some biologist's fractal properties of DNA can be used to resolve evolutionary relationships in animals.

Perhaps in the future biologists will use the fractal geometry to create comprehensive models of the patterns and processes observed in nature.

1.2.3 Fractals in computer graphics

The biggest use of fractals in everyday live is in computer science. Many image compression schemes use fractal algorithms to compress computer graphics files to less than a quarter of their original size.

Computer graphic artists use many fractal forms to create textured landscapes and other intricate models.

It is possible to create all sorts of realistic "fractal forgeries" images of natural scenes, such as lunar landscapes, mountain ranges and coastlines. We can see them in many special effects in Hollywood movies and also in television advertisements.

The "Genesis effect" in the film "Star Trek II - The Wrath of Khan" was created using fractal landscape algorithms, and in "Return of the Jedi" fractals were used to create the geography of a moon, and to draw the outline of the dreaded "Death Star".

But fractal signals can also be used to model natural objects, allowing us to define mathematically our environment with a higher accuracy than ever before.

Figure 1.8 - A fractal landscape

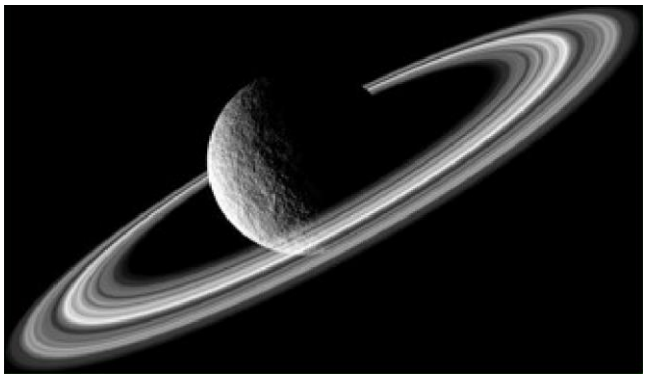

Figure 1.9 – A fractal planet

1.3 Fractal Dimension as a quantitive parameter of regular structures

To quantify fractals, the Hausdorf-AS dimension can be used. . For fractals, the Hausdorff-Bezikovich dimension usually takes fractional values ("fractus" - "fractional") and its larger topological dimension.

The Hausdorf-Bezikovich dimension allows the number to measure the degree of undulation, inhomogeneity, or instability of an object. It increases as the ripple

increases, while the topological dimension does not take into account all the changes that occur with a line or surface, unless they are accompanied by rupture or gluing of some points.

There are also more abstract ways to determine the dimension. Suppose a segment of straight line length of 1 centimeter. In order to cover a straight line with segments 1 \ 10 cm long, you need 10 segments. To cover a square with a side of 1 cm, you need one hundred squares with a side of 1 \ 10 cm. A cube with an edge length of 1 cm can be covered with a thousand cubes with an edge of 1 \ 10 cm. Thus, the dimension appears in exponents: 10^1, 10^2, 10^3.This sequence does not depend on the scale selected to measure the segment, the side of the square, or the edge of the cube.

Important: A geometric object is characterized by the minimum number of cells needed to cover the object. Denote the exponent in the above ratios D, the number of "cells" N, and the size of the "cell" δ. Then from the examples considered by us we will receive expression $N=(1/\delta)^D$. We logarithm both parts of the equation and get:

$$\log N=D\log(1/\delta), \quad \rightarrow \quad D=\log N/\log(1/\delta). \quad (1.10)$$

A classic example of determining the fractal dimension of real objects is determining the length of the shoreline. To measure the length of the shoreline, the map is covered with a grid. Let the square cells of the grid have dimensions δ x δ. Number N (δ) such cells required to cover the shoreline on the map is approximately equal to the number of steps that can be bypassed on the map of the shoreline with a compass with a slope δ. Reduction of δ leads to an increase in the number of cells required to cover the shoreline.

If the shoreline had a well-defined length L_N, then one would expect the number of steps of a compass or the number of square cells N(δ), and magnitude L(δ)=N (δ) x δ when decreasing δ will strive for a permanent L_N.

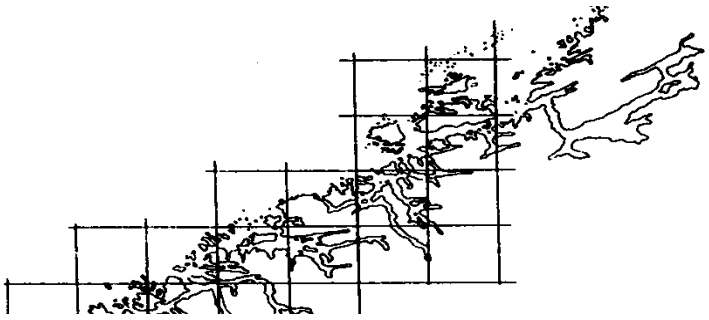

Figure 1.10 - Cover the shoreline with a grid to determine its length

However, as can be seen from Figure - 1.6, while reducing the length δ step measured length increases. A graph constructed on a double logarithmic scale shows that when decreasing δ the measured length of the shoreline is described by the approximate formula:

$$L(\delta) = a\,\delta^{1-D} \qquad (1.11)$$

For a normal curve $a=L_N$ (with sufficiently small δ) and the value of D is equal to one. But for the coastline, as seen in the graph, D≈1,52. Thus, the shoreline is a fractal with fractal dimension D.

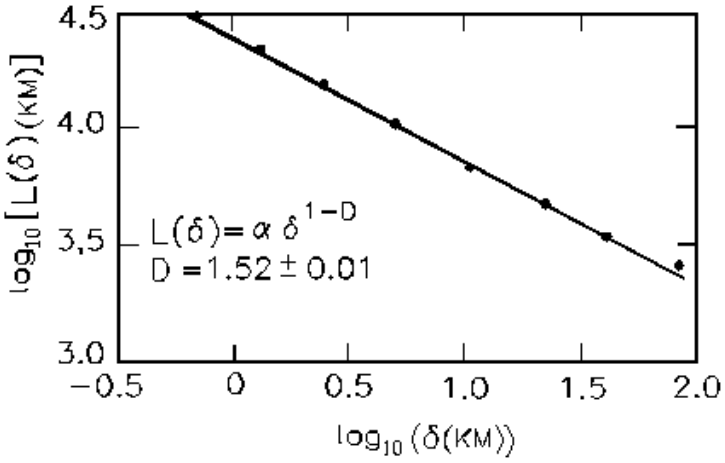

Figure 1.11 - The dependence of the length of the shoreline on the side length δ of the cells of the applied grid.

One of the main properties of fractals is self-similarity, ie their appearance does not change significantly when viewed under a microscope with any magnification.

In the simplest case, a small part of a fractal has information about the whole fractal.

There are geometric or regular fractals (Cantor's set, Koch's Figure -, Serpinsky's triangle and blanket, etc.) and natural, natural fractals (colloidal aggregates, clouds, polymers, porous media, dendrites, cracks, surfaces of cracks in solids, etc.). .

Regular (geometric) fractals are constructed by the method of iterations.

The main property of fractal sets is their self-similarity. However, natural fractal structures are not strictly self-similar, they are statistically self-similar (self-affine) objects.

The difference between these concepts is that for self-affiliated objects, the similarity coefficients differ by different dimensions. The fractal dimension for self-affine structures is not precisely determined, but is estimated by indirect calculations.

Traditional methods of geometry, which are widely used in the natural sciences, including materials science and mechanics of deformable bodies, are based on an approximate approximation of the structure of the object under study, geometric Figure -s - lines, segments, planes, polygons, polyhedra, spheres. In this case, the internal structure of the object under study is usually ignored, and the processes of formation of structures and their interaction with the environment are characterized by integral thermodynamic parameters.

This leads to the loss of much of the information about the properties and behavior of the systems under study. Euclidean dimensions can serve as characteristics of symmetric microstructures, which are infrequently formed even in materials obtained under quasi-equilibrium conditions.

Therefore, the application of fractal theory allows the introduction of new quantitative indicators of structures in the form of fractal dimensions. This is the basis for modeling structures of various natures.

Conclusion to the part 1

Based on the results of the review of the presented methods, the following main conclusions can be drawn:

Fractal Dimension is a concept when applied to abstract geometric fractals such as the Sierpinski Triangle and the Menger Sponge.

Many scientists have found that fractal geometry is a powerful tool for uncovering secrets from a wide variety of systems and solving important problems in applied science.

The list of known physical fractal systems is long and growing rapidly. Fractals improved our precision in describing and classifying "random" or organic objects, but maybe they are not perfect. Maybe they are just closer to our natural world, not the same as it.

Some scientists still believe that true randomness does exist, and no mathematical equation will ever describe it perfectly. So far, there is no way to say who is right and who is wrong. Perhaps for many people fractals will never represent anything more than beautiful pictures.

The aim of the investigation of the master thesis are:

1. To substantiate the possibility of applying the methods of fractal geometry when monitoring the fatigue damage of clad aluminum alloy D16AT by studying the deformation relief at the meso level.

2. To develop a method of automated determination of fractal dimensions of deformation relief on surface images obtained by optical microscopy.

3. Investigate the evolution of the deformation relief of the surface of optical microscopy and establish the relationship between fatigue damage of a structural element and its fractal dimension.

2 METHODOLOGY OF THE DEFORMATION REIEF ESTIMATION BY THE FRACTAL DIMENSION

2.1 Introduction

A necessary component of the process of creating aircraft is fatigue testing of materials, structural elements, full-scale resource testing of structures. Full scale tests - the stage, which requires significant material costs, is long and responsible. Field tests allow to determine the places of potential fatigue failure of structures, to justify their resource. Identifying areas of fatigue crack formation in the early stages of damage helps to reduce the duration of tests and increase the reliability of aircraft.

One of the instrumental methods of the metal fatigue diagnostic is nondestructive method based on the light microscopy investigation of the deformation relief, formed on the surface of aluminum alloy under fatigue. Deformation relief originated on the surface of alclad aluminum alloy under cyclic loading. As a result of aluminum alloy cyclic loading we can see the signs of microplastic deformation - the system of extrusions and intrusions, persistence slip bands. By the usage of light microscopy, the signs of deformation (deformation relief) are presented like black (deformed area) and white (not deformed area) clusters. The damage parameter was taken like quantitative parameter of deformation relief. Damage parameter is the ratio of black area (with the signs of microplastic deformation) to the total area of the investigated zone. At the department of Aircraft Design this investigation was taken as the base of methods for the evaluation of the fatigue damage of aviation structure elements.

2.2 Object of the investigation. Materials and specimens.

The object of the investigation is the deformation relief obtained on the surface of aluminum alloy. Fatigue tests with optical monitoring and calculations of quantitative parameters of deformation relief were performed at the National Aviation University.

Aluminum alloy D16AT remains one of the most common structural materials in the manufacture of aircraft structures. Despite the increasing introduction of composite materials, the modern Ukrainian aircraft AN-140, AN-148 are made of D16AT alloy. As for foreign aircraft, it should be noted that in their designs are widely used alloy 2024 T3, which in its composition and mechanical characteristics is analogous to the alloy D16AT.

In this regard, as well as due to the possibility of observing the processes of formation and development of deformation relief on the surface of the clad layer under cyclic loading, the alloy D16AT was chosen for the study.

D16AT alloy has a tensile strength of 405 MPa, yield strength of 270 MPa, maximum elongation of 13%, modulus of elasticity of 71 MPa. In addition to aluminum, this alloy contains: Copper - 3.8 - 4.9%, magnesium - 1.2 - 1.8%, manganese - 0.3 - 0.9%. To protect against corrosion, the D16AT sheet alloy is clad with aluminum. The thickness of the weeping layer is 5-7% of the thickness of the sheet.

It is the weeping layer, according to the main idea of the presented work, is a carrier of information about the accumulated fatigue damage.

The main volume of experiments was performed on samples of sheet clad alloy D16AT, the geometry of which is shown in Fig. 2.1. To localize the damage and the control area, the samples have a stress concentrator in the form of a hole.

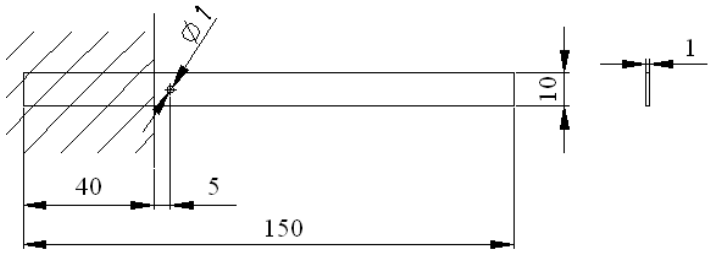

Figure 2.1 - Sample for fatigue tests under cantilever bending.

The tests were performed on a machine (Fig. 2.4), which allows to load compact samples by cyclic bending with a frequency of 25 Hz in a wide range of load amplitudes and asymmetries of the load cycle.

The amplitude of deformations and corresponding stresses is determined by the eccentricity of the axis of attachment of the connecting rod (7) to the flywheel (8) or the length of the working part of the sample, which can be adjusted accordingly. The asymmetry of the cycle can be set by the position of the slider (6).

To ensure the scientific and practical value of the presented research it was decided to provide as much as possible the similarity of the test conditions to the real loading conditions of the plane structures and to select materials actually used in aviation industry.

As the material for the specimens the aluminum alloys D16AT has been selected. This material is widely used for the aircraft skin manufacturing.

Table 2.1 - Chemical composition of the aluminum D16AT alloy.

Component	Wt. %	Component	Wt. %	Component	Wt. %
Al	90.7 - 94.7	Mg	1.2 - 1.8	Si	Max 0.5
Cr	Max 0.1	Mn	0.3 - 0.9	Ti	Max 0.15
Cu	3.8 - 4.9	Other, each	Max 0.05	Zn	Max 0.25
Fe	Max 0.5	Other, total	Max 0.15		

Table 2.2 - The physical properties of aluminum D16AT alloy.

Properties	**Metric**	**Imperial**
Density	2.78 g/cm^3	0.1 lb/in^3

To protect sheets of alloy used for the fuselage skin against corrosion they are covered by pure aluminum. The so called clad layer being easily plastically deformed serves as a fatigue damage indicator.

Table 2.3 - The mechanical properties of aluminum D16AT alloy.

Properties	**Metric**	**Imperial**
1	2	3
Hardness, Brinell	120	120
Hardness, Knoop	150	150
Hardness, Rockwell A	46.8	46.8
Hardness, Rockwell B	75	75
Hardness, Vickers	137	137
Ultimate Tensile Strength	483 MPa	70000 psi
Tensile Yield Strength	345 MPa	50000 psi

End of the Table 2.3

1	2	3
Elongation at Break	18 %	18 %
Modulus of Elasticity	73.1 GPa	10600 ksi
Notched Tensile Strength	379 MPa	55000 psi
Ultimate Bearing Strength	855 MPa	124000 psi

Bearing Yield Strength	524 MPa	76000 psi
Poisson's Ratio	0.33	0.33
Fatigue Strength	138 MPa	20000 psi
Machinability	70 %	70 %
Shear Modulus	28 GPa	4060 ksi
Shear Strength	283 MPa	41000 psi

For the fatigue tests the smart specimens were used (fig.2.2). The specimens are made from alclad aluminum alloy D16AT with the thickness in 1,2 mm.

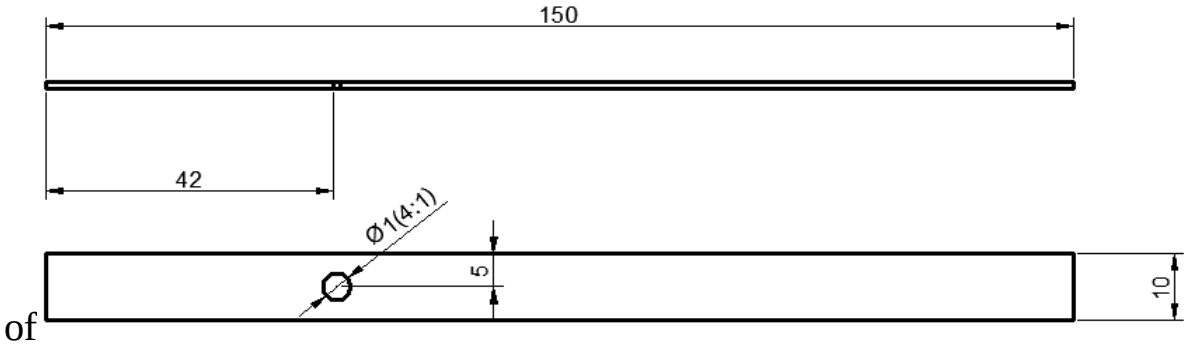

of

Figure 2.2 - Geometry of the specimen for the fatigue test.

The base material is covered by pure aluminum to protect from the corrosion. The surface of this layer is sensitive to plastic deformation, so the deformation relief is initiated on the surface. All specimens were subjected to the bending loading at small test machine.

Mechanical polishing was conducted to provide correct light microscope surface analysis. The diamond paste of 3-4 micro meter grain grade was used for the polishing.

The surface state after polishing is shown in the fig. 2.3.

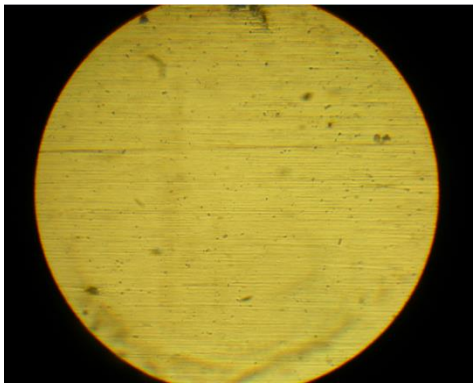

Figure 2.3 - The image of the specimen surface after the polishing with diamond paste. Magnification 300 ^{x} .

2.3 Equipment for the investigation

For the fatigue loading the special test machine designed in the research laboratory of Aircraft Design Department has been used. The scheme of the machine is shown in Fig. 2.4.

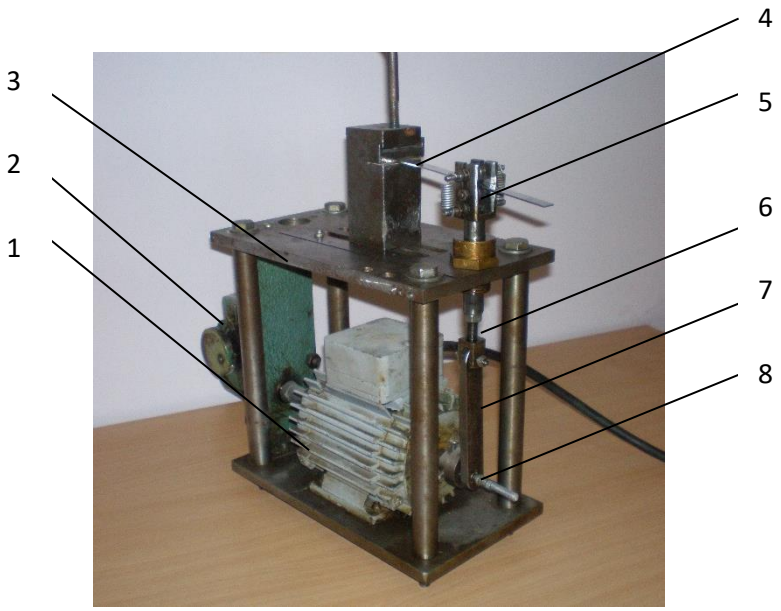

Figure 2.4 - Special machine for fatigue tests: 1 – electromotor, 2 – cycles gauge, 3 – machine frame, 4 – specimen for fatigue tests, 5 – grip for specimen, 6 – slider, 7 – connecting rod, 8 – flywheel.

The machine consists of 20 mm steel plate which is serves as a basis for fixing the construction elements of the machine. Electric motors and cycles gauge and four columns which bear sample fixator components, are mounted on plate.

The level of stress in the working section of the specimens is determined by the formula:

$$\sigma \frac{3E \cdot y \cdot x \cdot b}{2 \cdot l^3} \max \square \qquad (2.1)$$

where:

E – modulus, kg/mm^2;

y – the length used from the concentrate hole, mm;

x – amplitude of the specimen, mm;

b – thickness of the specimen, mm;

l – the total used length, mm.

In this experimental series, two modes of tests have been conducted, so we set two arrangements for the machine, the first is only for the bending (Fig. 2.4), the second one for the combining loading by bending and torsion (Fig. 2.5). The 3D “Inventor” and “Solid Works” software for the drawing presentation have been used along the work.

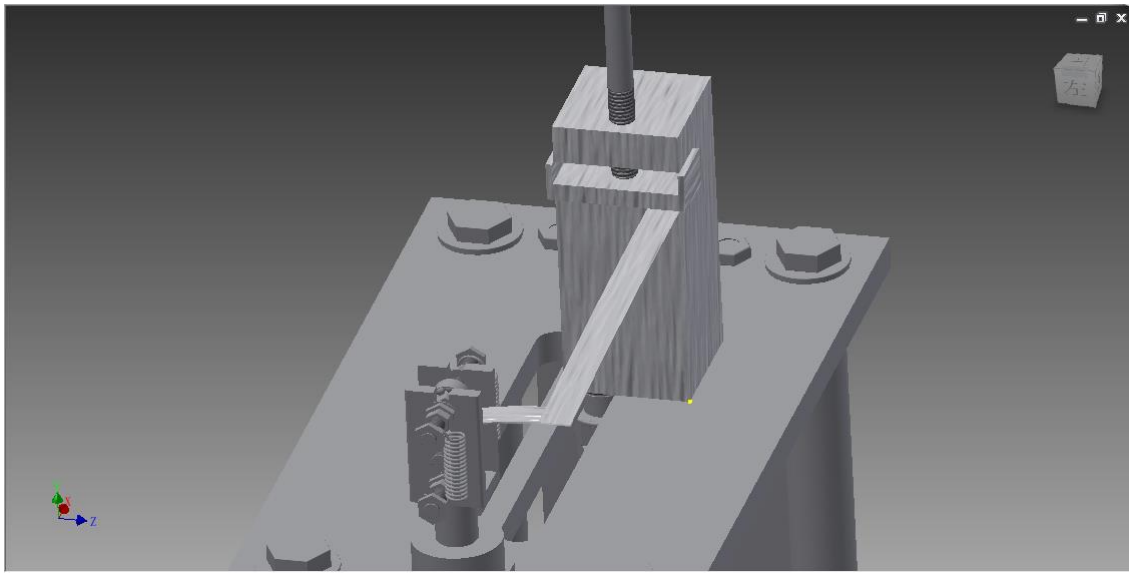

Figure 2.5 - 3D “Inventor” image of the machine for combining loading by bending and torsion.

The specimen is being loaded by the loading carriage actuated by the slider. The pull-push motion of the slider provided by the connected rod. The stress ratio can

be altered by the position of the screw for the stress ratio adjustment. The longer specimen the less stress arises in the cross sections.

The sample on the one side is fixed in the grip. Another side of the specimen attached to the torque level. The free side of lever is situated between two ball bearings which are forced to the lever by the springs. This lever provides combined bending and torsion loading of the specimen.

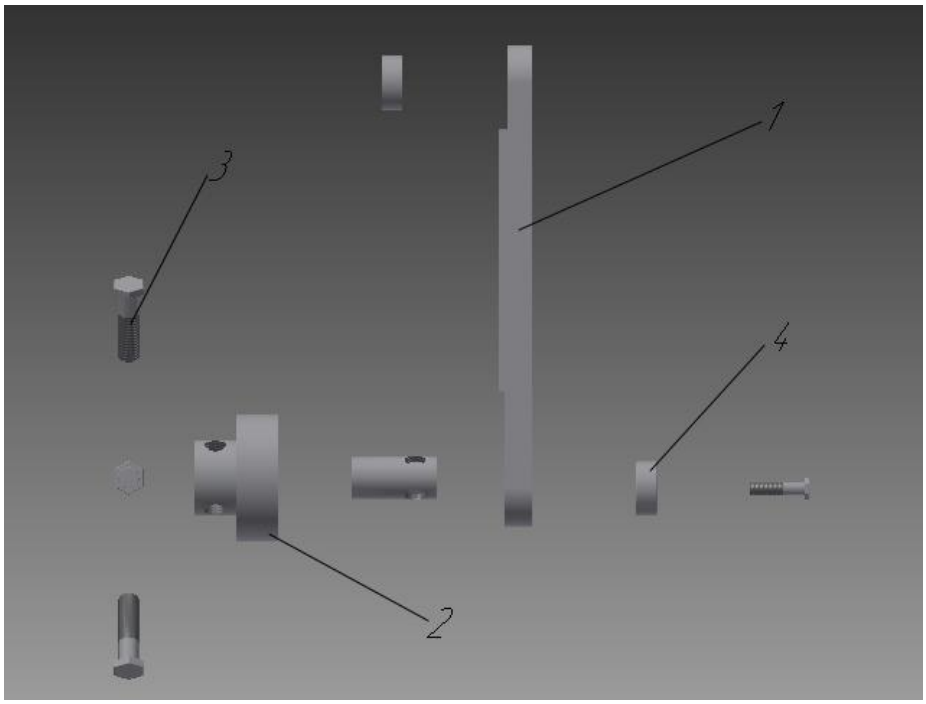

Figure 2.6 - 3D “Solid Works” images of some components of the machine for the biaxial cyclical loading: 1) connecting rod; 2) flywheel; 3) fixed screws; 4) ball bearing.

The light microscope METAM P-1 with magnification of 300-500 times to observe the specimens surface state was used (Fig. 2.7).

Figure 2.7 - The light microscope METAM P-1.

The photos were taken by Olimpus FE-190 camera, fitted to the microscope.

Cyclic loading modes are selected taking into account the loading conditions of real aircraft structures. In this case, given that the clad aluminum alloy D16AT is traditionally used for the manufacture of fuselage cladding, it is the conditions of loading the fuselage with excess pressure were modeled, mainly in fatigue tests.

In flight and on the ground the plane is subjected to wide spectrum of loads, as a result of these the normal and shear stresses occur. The bending loading has been selected as a primary cause of fatigue damage accumulation.

2.4 Application of Finite Element Method for stress-strain analysis.

For the Finite Element Method analysis the Autodesk Inventor 2013 software has been used.

Below, principle steps of the procedure are presented as a set of 3D images. Analysis includes bending mode of loading fig.2.8-2.12.

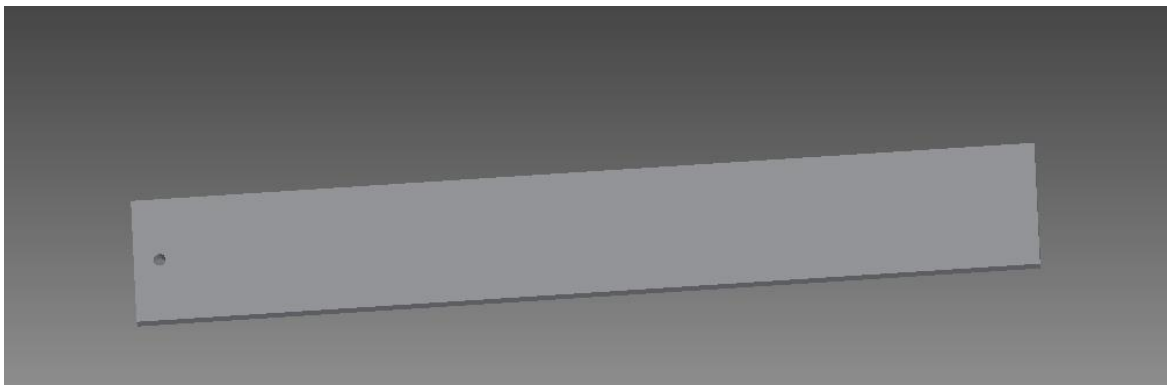

Figure 2.8 - Step 1 of the bending analysis: 3D “Inventor” model of the 10mm×1mm×100mm specimen with a 1.0 mm hole.

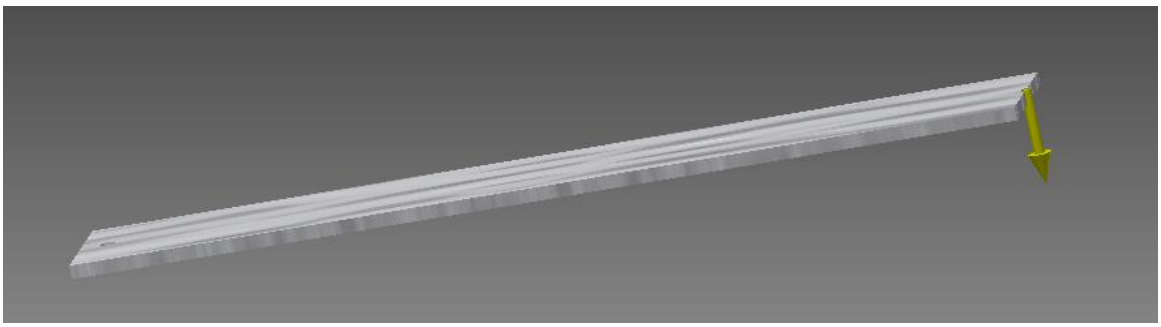

Figure 2.9 - Simulation of the load applied at the edge of the specimen.

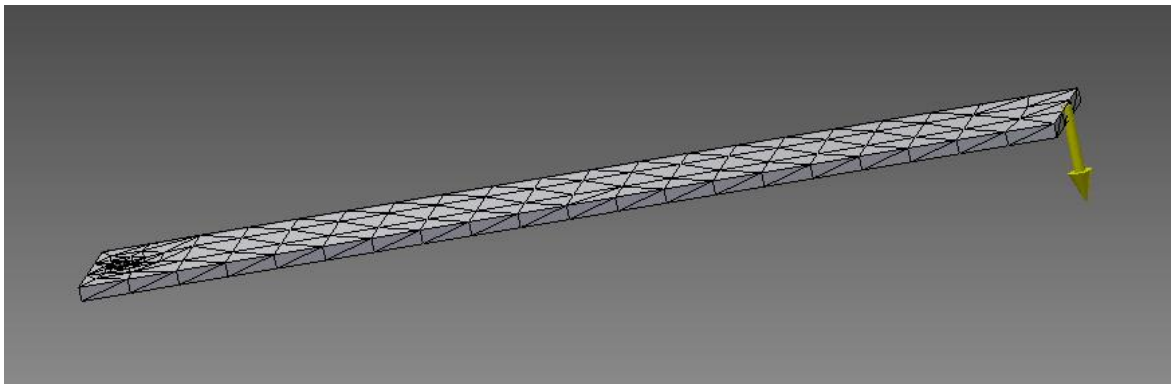

Figure 2.10 - Specimen with finite element mesh.

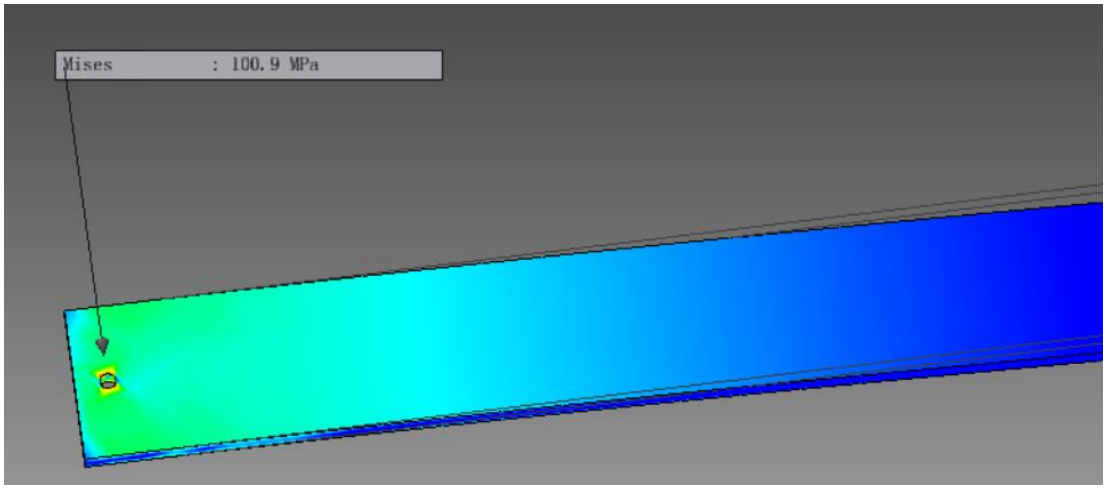

Figure 2.11 - Stress analysis nearby the hole.

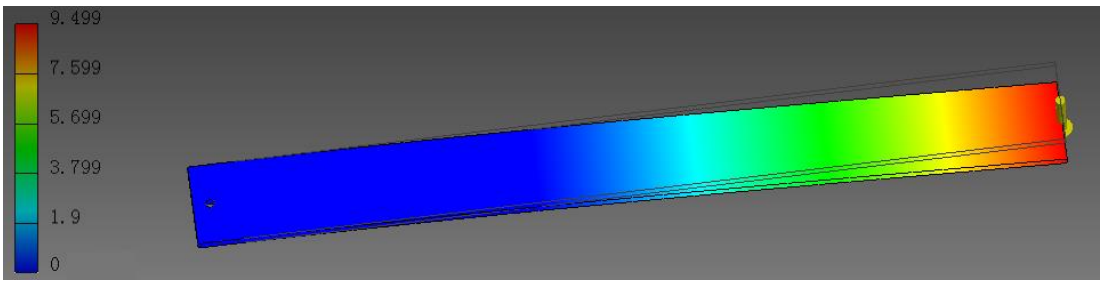

Figure 2.12 - Free edge displacement assessment for the required stress.

As a result of Finite Element stress-strain analysis desirable levels of stresses under the two modes of loading have been achieved by the correct selection of specimen length, displacement, and twist.

The stresses at the inspected area were established to be close to the operational level for the aircraft components.

2.5 The algorithm of the experiment

Main steps of the experiment are shown in the algorithm (Fig. 2.13).

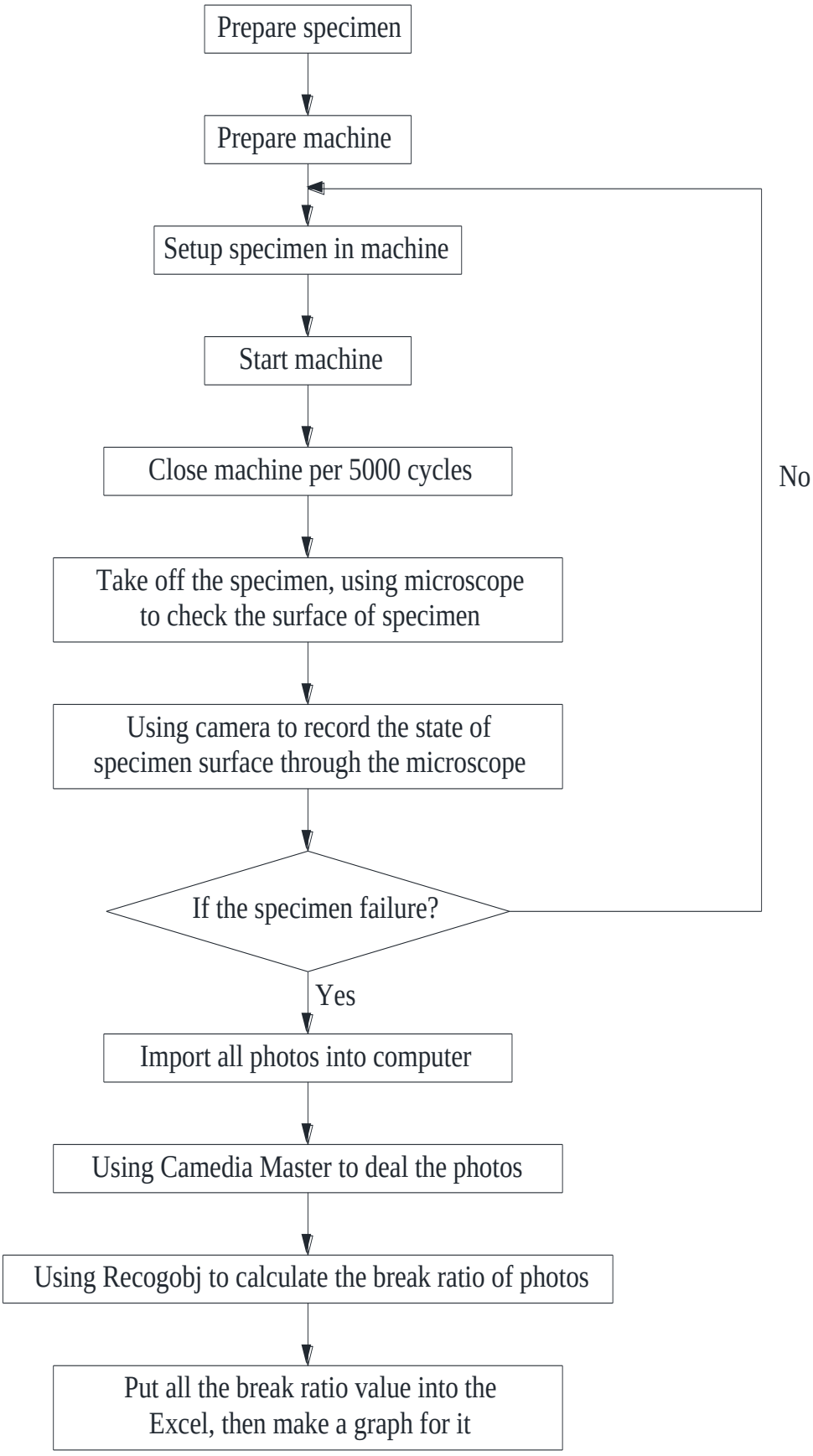
Prepare specimen
Prepare machine
Setup specimen in machine
Start machine
Close machine per 5000 cycles
No
Take off the specimen, using microscope to check the surface of specimen
Using camera to record the state of specimen surface through the microscope
If the specimen failure?
Yes
Import all photos into computer
Using Camedia Master to deal the photos
Using Recogobj to calculate the break ratio of photos
Put all the break ratio value into the Excel, then make a graph for it

Figure 2.13 - The algorithm of the experiment

2.6 Images analysis

The analysis of digital images and assessment of the damage after the certain number of cycles was performed by the procedure developed at the Aircraft Design Department of National Aviation University.

The key idea of the mentioned procedure is calculation of the part of the surface area with the signs of localized plastic deformation. In fact, these signs are extrusion/intrusion structures proved to be indicators of accumulated fatigue damage (fig.2.14).

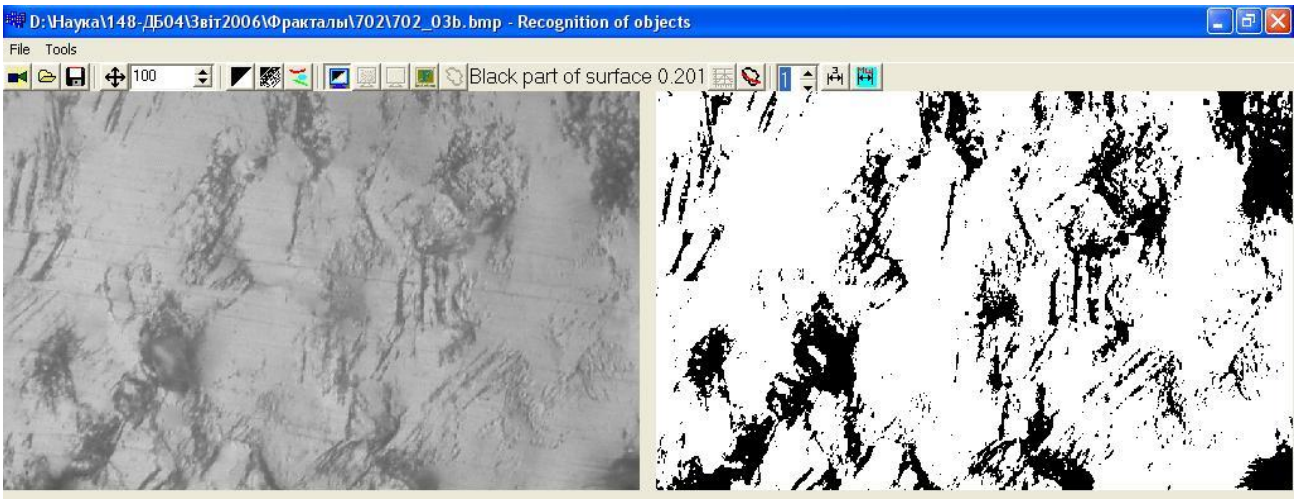

Figure 2.14 - Separation of the black and white area on the surface of specimen for the calculation of accumulated damage.

Conclusion on the part 2

The part 2 deals with the substantiation of experimental procedure. It comprises selection of material for the specimens, description of the modes and levels of stresses for the real aircraft components loading simulation, procedures for the data analysis.

The object of research was selected Aluminum alloy D16AT. This alloy one of the most common structural materials in the manufacture of aircraft structures and widely used for the aircraft skin manufacturing. The main volume of experiments was performed on samples of sheet clad alloy D16AT. All specimens were subjected to the bending loading at small test machine. For the fatigue loading the special test machine designed in the research laboratory of Aircraft Design Department has been used.

In this experimental series, two modes of tests have been conducted, so we set two arrangements for the machine, the first is only for the bending, the second one for the combining loading by bending and torsion.

As a result of Finite Element stress-strain analysis desirable levels of stresses under the two modes of loading have been achieved by the correct selection of specimen length, displacement, and twist.

3 FRACTAL GEOMETRY APPLICATION FOR THE FATIGUE DAMAGE MONITORING OF D16AT STRUCTURAL ALLOY

The possibility of using fractal geometry methods in the problem of fatigue stress assessment on the surface condition is determined by the fractal nature of the deformation relief.

3.1 Fractality of the deformation relief clusters

The deformation relief is a three-dimensional structure that is formed and developed under the action of cyclic loading on the surface of the alcladding alloy D16AT.

As can be seen from the images of the deformation relief obtained by light microscope (Figure 3.1 a) and scanning electron microscopes (Figure 3.1 b), the relief clusters, which are the result of the formation of extrusions and intrusions, are irregular, which does not allow describe their shape by methods of traditional geometry.

By the nature of the formation, the deformation relief is a self-organized irregular structure, along with its visual signs of self-similarity, this gives reason to believe that the deformation relief is a natural fractal.

For natural fractals, there is a large-scale restriction on their existence, the maximum and minimum size at which they meet the fractality criteria, including the fractional dimension.

The fractal dimension of the deformation relief in the presented work is determined by manual and automated calculations by the method of "box-counting".

This manual calculation allowed to make a preliminary conclusion - for the analysis of structures formed by the action of cyclic loading on the surface of the structural aluminum alloys, fractal geometry methods can be used.

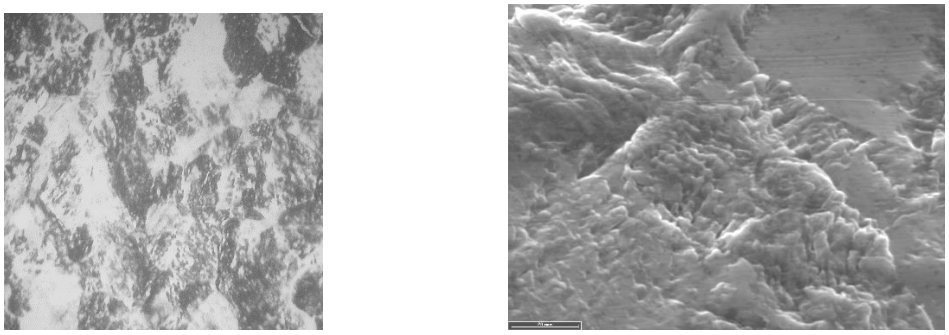

a) b)

Figure 3.1 - Images of the deformation relief surface obtained by:
a) light microscope (x 350);
b) scan microscope (x 2000).

In Figure 3.2 presents an image of the deformation relief of the surface of the aluminum alloy D16AT, obtained by light microscope MMP-4 at a magnification of 300 times after 65,000 load cycles with a maximum stress of 100.0 MPa, R = 0.

Let's create a grid of boxes, we will impose it on the image of a deformation relief. The size of the box д is assumed to be equal to 5 pt (Figure 3.2 a), 8 pt (Figure 3.2 b), 11 pt (Figure 3.2 c), 14 pt (Figure 3.2 d), 17 pt. 3.2 e), 20 pt (Figure 3.2 e). For the accepted sizes we will count quantity of boxes N (δ) covering contours of clusters of a deformation relief. The results of the calculations are entered in table. 3.1. The graph of the dependence of log N (δ) on log 1 / δ (Figure 3.3) allows us to determine the fractal dimension of the contours of the clusters of the deformation relief, or the dimension along the perimeter D_p. Experimental data can be approximated by a linear equation: logN (δ) = 1,1399log1 / δ + 3,8073. The angle of inclination of the approximated line determines the fractal dimension. As can be seen, for the current state of the surface and the corresponding accumulated damage Dp = 1.14.

The high value of the coefficient of determination $R^2 = 0.98$ when applying the equation logN (δ) = 1,1399log1 / δ + 3,8073 indicates the validity of the assumption about the fractal nature of the surface defective structures under study.

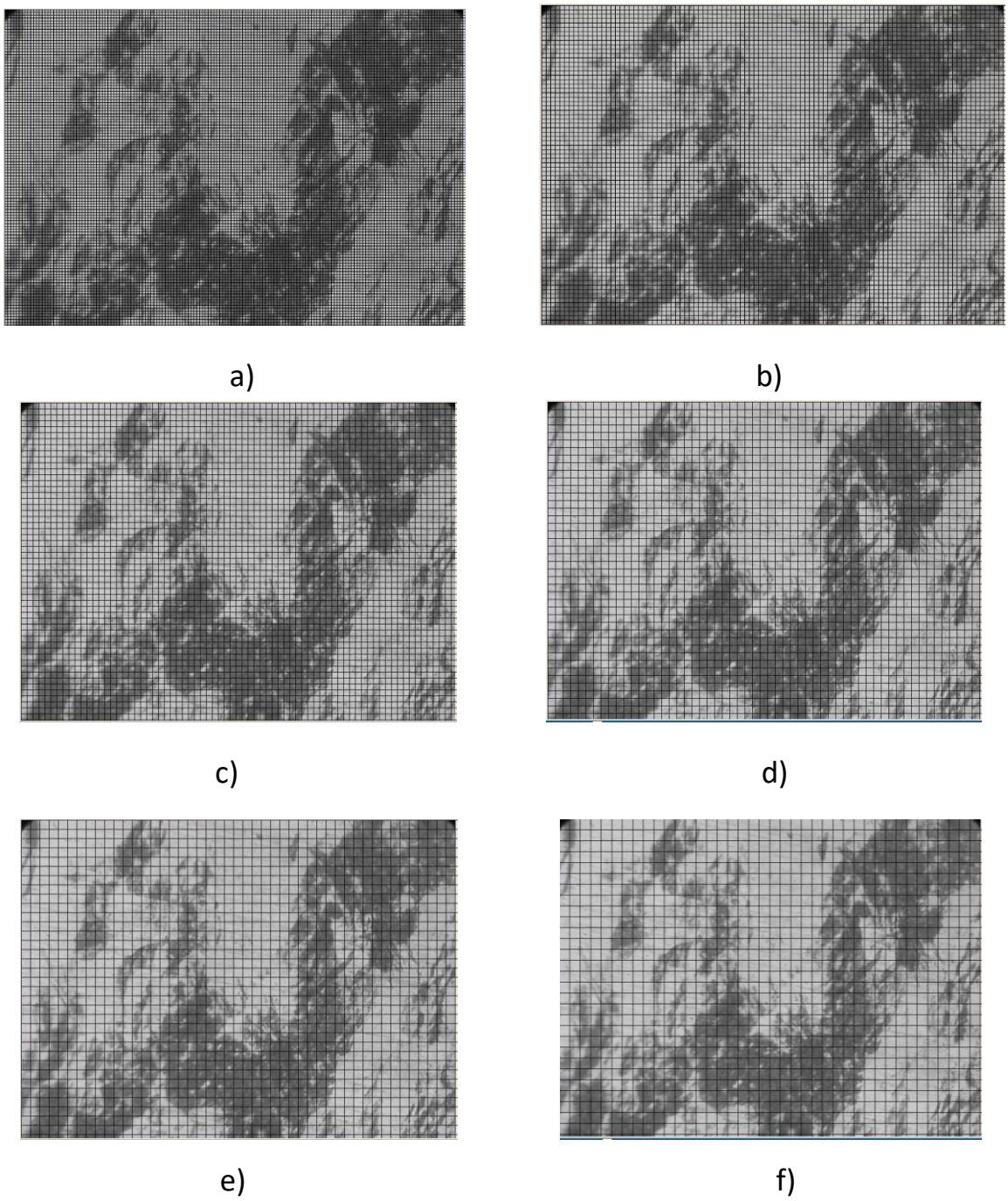

Figure 3.2 - Coating of the surface deformation structure with a large-scale grid with the size of the boxes: a) 5pt, b) 8pt, c) 11pt, d) 14pt, e) 17pt, f) 20pt.

Table 3.1 - The results of counting the number of cells covering the perimeter of the clusters of deformation relief, depending on the size of the cells

δ, pt	N(δ)	log N(δ)	1/ δ, пт$^{-1}$	log (1/ δ)
5	962	2,98	0,2	-0,699
8	558	2,747	0,125	-0,903
11	471	2,673	0,09	-1,041
14	365	2,562	0,071	-1,146
17	254	2,405	0,059	-1,23
20	200	2,301	0,05	-1,301
23	191	2,281	0,043	-1,362
26	159	2,201	0,038	-1,415
29	120	2,079	0,034	-1,462

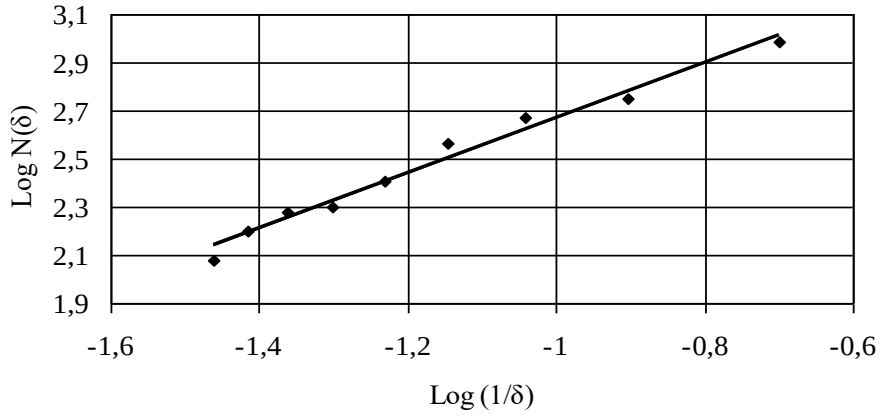

Figure 3.3 - Graph of the dependence of the number of cells covering the contours of clusters of deformation relief on the value inverse of the size of the side of the cell.

At the next stage of work after determining the fractal dimension of the contours of the relief clusters by manual calculation, special software for automated

calculations was developed. The program is based on previously developed software for calculating the damage parameter D, which determines the saturation of the surface with traces of microplastic deformation.

The values of fractal dimensions were obtained by automated calculation D_S, D_P, $D_{P/S}$.

The corresponding fractal dependences are presented in Figure 3.4 –3.6. The deformation relief after 400,000 loading cycles was analyzed, at the maximum stress of the loading cycle of 125.6 MPa and the asymmetry coefficient R = 0.

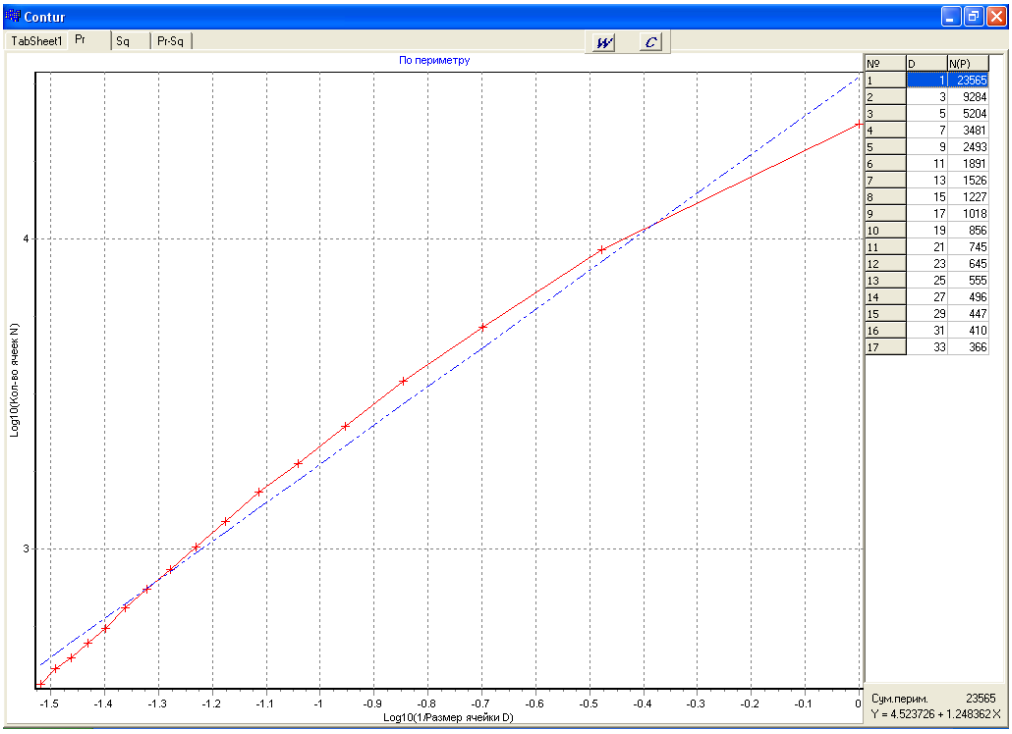

Figure 3.4 - Dependence of the number of cells covering the contours of clusters on the size of cells (program window).

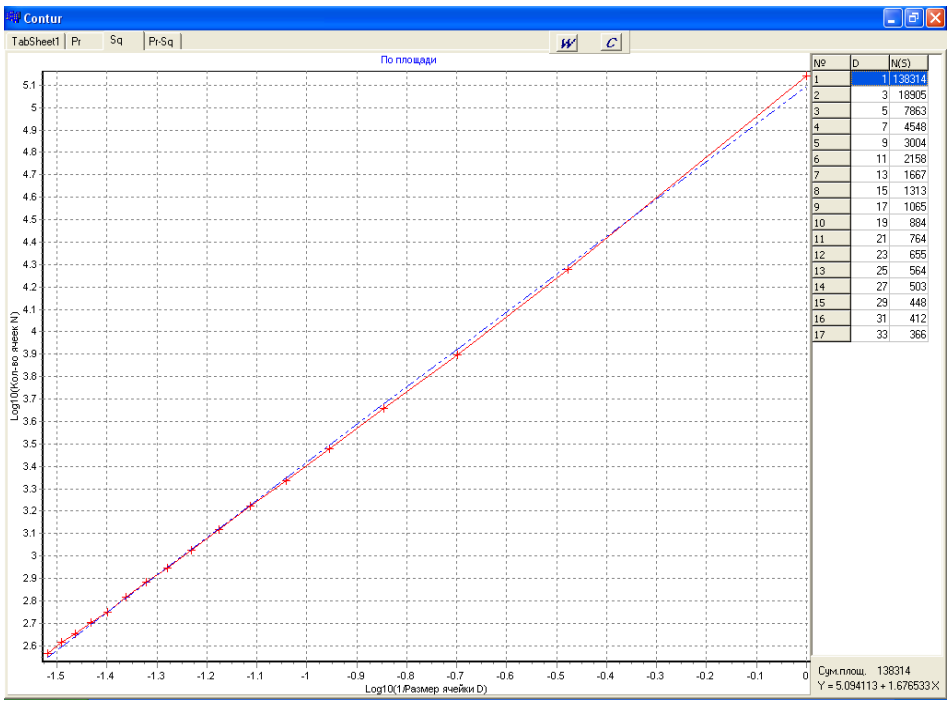

Figure 3.5 - Dependence of the number of cells covering the surface of clusters on the size of cells (program window).

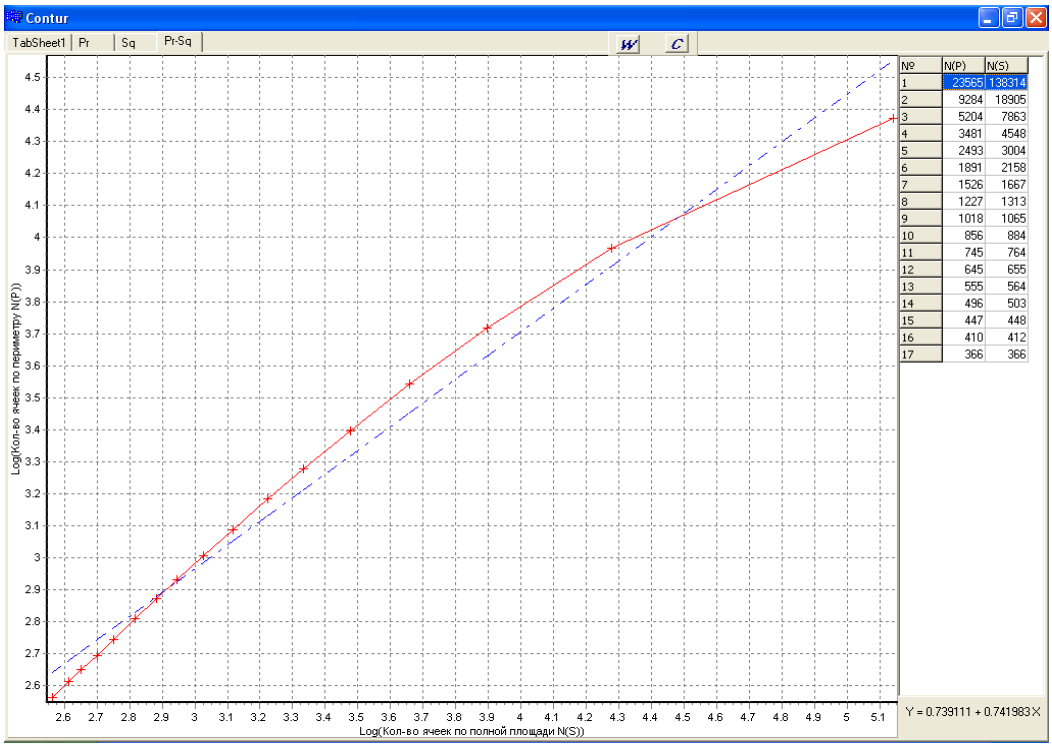

Figure 3.6 - Relationship of the number of cells covering the contours of clusters with the number of cells covering the surface of clusters (program window).

The size of the cells δ ranged from 2 pt to 34 pt in steps of 2 pt.

Further increase in the size of the cells was impractical due to the fact that the cells of a certain size cover the surface of the cluster of the deformation relief as a whole and the scale of the calculation in this case can not affect its result. Thus, the size of the cells is more than 34 pt exceeds the allowable scale range of fractal analysis.

In the table. 3.2. the results of correlation analysis of the dependences lnNs = f (ln1 / δ) are given; lnNp = f (ln1 / δ); lnNp = f (lnNs) at their linear approximation and fractal dimensions are defined. For dimensions Ds and Dp, these are the coefficients before the variable; for the dimension Dp / s, which is determined from the ratio of the perimeter to the area.

The fractal dimension is equal to twice the coefficient before the variable resulting from the ratio: $P \approx \sqrt{S^D}$. To determine the fractal dimension of clusters of deformation relief, we obtain: $P^2 = S^D \Rightarrow \Rightarrow D = \frac{2\ln P}{\ln S}$.

Since when determining the dimension by the method of "box-counting" both the contours (perimeter) and the surface (area) are covered with a grid of cells of size δ, the ratio $\frac{\ln P}{\ln S}$ can be replaced by the ratio $\frac{\ln N_P(\delta)}{\ln N_S(\delta)}$, where $N_P(\delta)$, $N_S(\delta)$ – the number of cells covering the perimeter of the cluster and the area, respectively. Therefore, the fractal dimension with respect to the perimeter to the area will be defined as the double tangent of the angle of inclination of the approximated curve $\ln N_P(\delta) = f(\ln N_S(\delta))$.

Table 3.2 - The results of correlation analysis of the dependencies that determine fractal dimensions of the deformation relief

Type of fractal dimension	Dp	Ds	Dp/s
Equations of approximating lines	y=4.5237+1.2484x	y=5.0941+1.6765x	y=0.7391+0.7419x
The value of the fractal dimension	1.25	1.68	1.48
Coefficient of determination, R^2	0.98	0.99	0.98

The obtained values of the coefficients of determination indicate the legitimacy of the assumption about the fractality of surface defective structures that are formed under cyclic loading.

As expected based on the analysis of known fractal structures of natural origin, the fractal dimensions of the contours of clusters of deformation relief, cluster surfaces, as well as fractal dimension, which was determined relative to the perimeter to area are in the range between one and two and exceed the topological dimension of the line.

Thus, it is proved that the deformation relief of polycrystalline aluminum, which is formed and developed under the action of cyclic loading, is a natural irregular fractal. The developed software made it possible to determine a number of fractal dimensions: fractal dimension of contours of clusters of deformation relief Dp, fractal dimension, which is determined by the area of clusters Ds and fractal dimension with respect to the perimeter to the area Dp / s.

The use of the fractal dimension of clusters of deformation relief makes it possible to quantitatively describe the relief to determine not only its saturation but also shape, both parameters change monotonically during cyclic loading, passing certain stages of accumulation of fatigue damage.

3.2 Selection of deformation relief parameters for assessment of accumulated damage and prediction of residual life

The choice of deformation relief parameters for the assessment of the accumulated damage and prediction of the residual resource is based on the results of fatigue tests with surface monitoring, correlation and regression analysis of the obtained data.

Test modes with monitoring of deformation relief in the process of cyclic loading were determined taking into account the stresses acting in real aircraft structures, as well as the results of previous studies and the corresponding fatigue curves.

Tests on cantilever cyclic bending and monitoring of the condition of the surface showed that even under load conditions that correspond to durability 10^7 cycles, on the surface of the weeping layer can be observed signs of deformation relief.

The choice of parameters for the models of forecasting the residual life on the deformation relief was carried out based on the results of tests of compact samples under stress σ_{max}=173,2 MPa, at cantilever from zero bending with control of a condition of a surface where tensile stresses acted.

In Figure 3.9 - Figure Figure 3.10 presents graphs illustrating the evolution of deformation relief parameters during loading in absolute and relative coordinates (σ_{max}=173,2 MPa, R = 0).

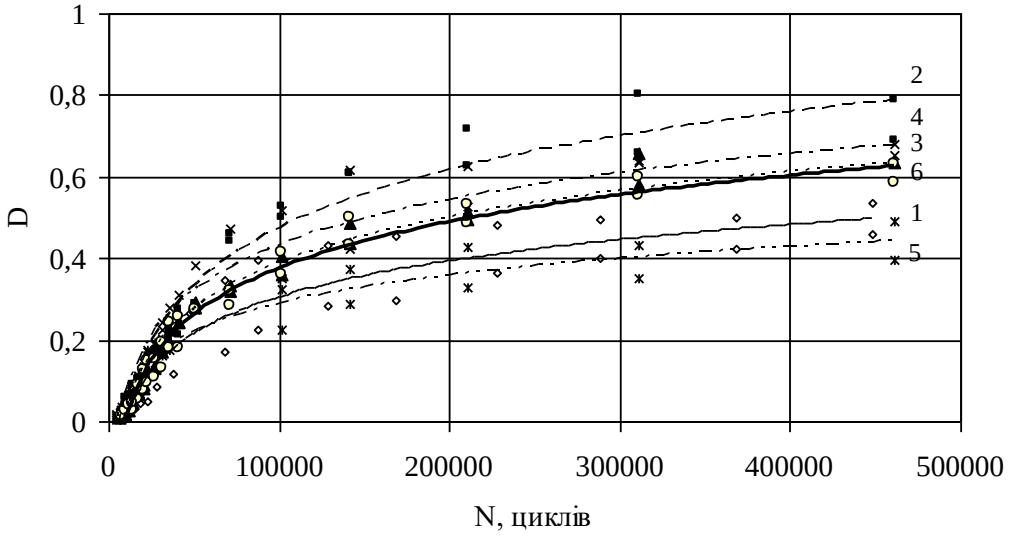

Figure 3.7 - Evolution of the damage parameter D (6 samples, σ_{max}=173,2 MPa).

The dependences of the previously proposed damage parameter on the number of load cycles are presented in Figure 3.9 in absolute coordinates.

In the future, taking into account the practical significance of estimating resource depletion and forecasting the residual number of load cycles, the results obtained on the change of deformation relief parameters are presented in the form N_{ov}%= f(D), N_{ov}%=f(Dp), N_{ov}%=f(Ds), $N_{ov,}$%=f(Dp/s).

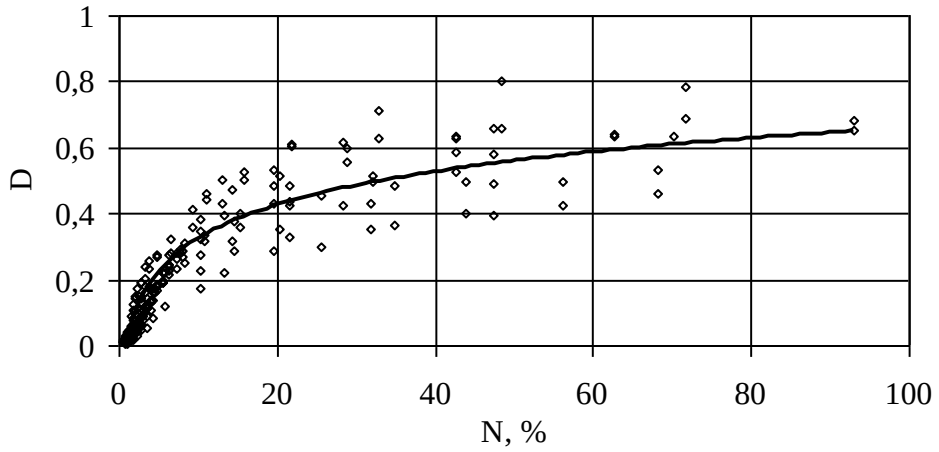

Figure 3.8 - Evolution of the damage parameter D.

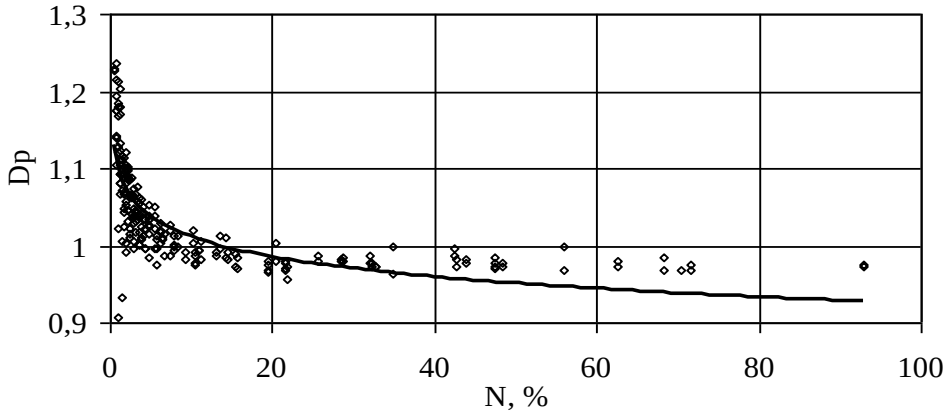

Figure 3.9 - Evolution of the fractal dimension Dp.

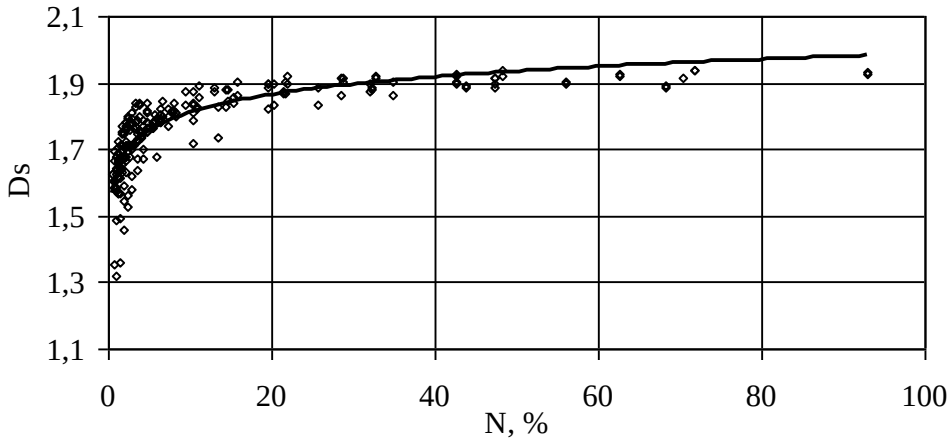

Figure 3.10 - Evolution of fractal dimension Ds.

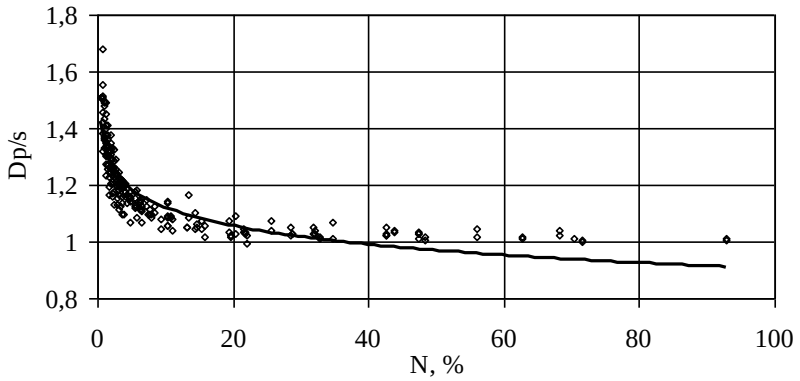

Figure 3.11 - Evolution of the fractal dimension Dp / s.

In the table. 3.3 presents the equation of approximating lines of dependences of the residual resource N_{ov}% from quantitative parameters of deformation relief: damage parameter D, fractal dimension of contours of relief clusters Dp, fractal dimension on the area of clusters Ds, fractal dimension in relation to the perimeter to the area Dp / s.

Table 3.3 - The results of experimental approximation data logarithmic curve

Dependence	Equation of approximating lines	Determination coefficient, R^2
N_{ov}%= f(D)	y=0,144Ln(x)-0,0107	0,88

End of the Table 3.3

N_{ov}%=f(Dp)	y=-0,037Ln(x)+1,0975	0,61
N_{ov}%=f(Ds)	y=0,0753Ln(x)+1,6361	0,71
N_{ov}%=f(Dp/s)	y=-0,0928Ln(x)+1,3365	0,79

Given the presence of a correlation between the number of load cycles and the above parameters of the deformation relief, the possibility of using multiple correlation models to estimate resource depletion is considered. Processing of experimental data was performed using Statgraphics Plus 5-0.

The results of regression and correlation analyzes are presented in table. 3.4.

Table 3.4 - Estimation of efficiency of application of parameters of deformation relief in models of forecasting of residual resource

Dependence	Модель	R^2
N_{ov}%=f(Dp/s)	N_{ov}%=-17,901+90,0103 Dp/s	37,04
N_{ov}%=f(D, Dp)	N_{ov}%=176,597-92,3604 D-64,5619 Dp	69,31
N_{ov}%=f(D, Dp/s)	N_{ov}%=180,346-109,588 D-56,6685 Dp/s	71,41

As can be seen from the above data, taking into account only the fractal dimension Dp / s does not provide sufficient accuracy of the forecast. At the same time, the application of the model N_{ov}%=180,346-109,588D-56,6685Dp/s, which is based on the values of the damage parameter D and the fractal dimension Dp / s, provides the largest value of the coefficient of determination.

The possibility of using type models is also considered N_{ov}%=f(D, Dp/s) for predicting residual durability under cyclic tensile loading.

It is known that the process of metal fatigue is staged. Stages are manifested at different scale levels. Thus, at the macro level we can distinguish the stage of fatigue crack formation and the stage of its propagation, in the study of microstructural transformations it is possible to identify certain stages associated with the formation of a number of dislocation structures, the process of changing micromechanical characteristics.

Analysis of the dependences of the selected parameters of the deformation relief on the number of loading cycles reveals the stages of development of the deformation relief.

Consider the dependences of the damage parameter D and the fractal dimension Dp / s on the number of load cycles obtained by testing samples tested at σ_{max}=173,15 MPa. The dependences presented in logarithmic coordinates allow to identify linear sections and their boundaries (Figure 3.14 - Figure 3.15).

Both dependences indicate a change in the speed of the studied processes with the same number of load cycles, which in this case is approximately 10% of the number of cycles before failure.

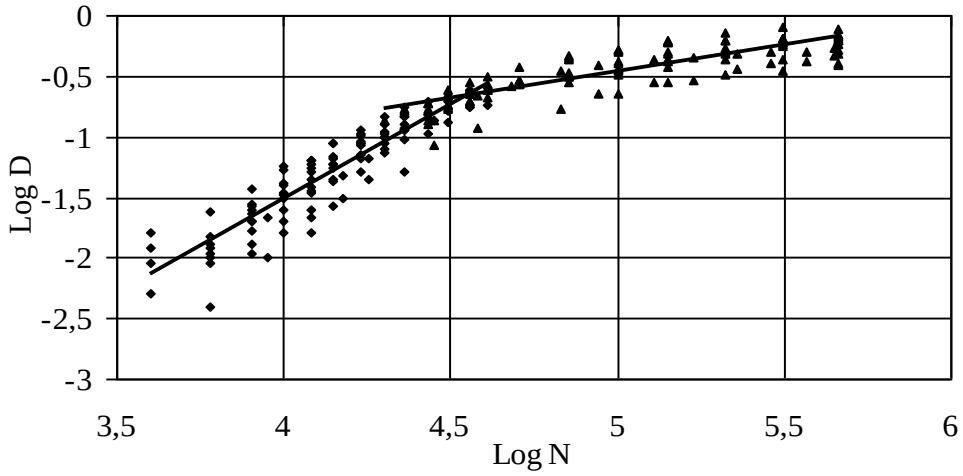

Figure 3.12 - Staged evolution of the damage parameter D.

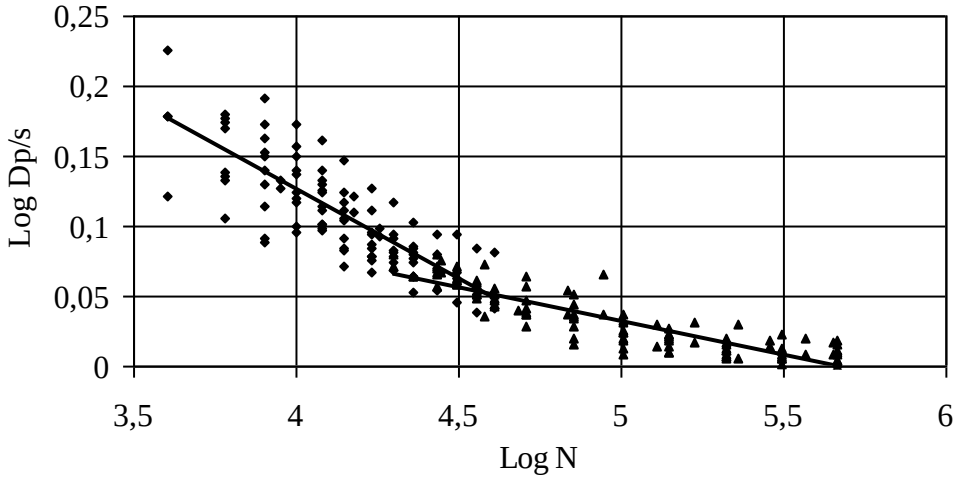

Figure 3.13 - Stages of evolution of the fractal dimension Dp / s.

The evolution of the damage parameter D is determined by a monotonic increase in the area of clusters of deformation relief during cyclic loading. The evolution of the fractal dimension Dp / s reflects the change in both the shape and area of the clusters, while the fusion of clusters of deformation relief leads to a decrease in the ratio of the perimeter of the clusters to their area.

On the graph of the dependence of the damage parameter D and the fractal dimension Dp / s on the number of loading cycles, two stages can be distinguished: The first stage is the stage of rapid growth of the number and area of clusters of deformation relief; the second stage is the stage of saturation, ie slowing down the process of attracting new grains in the process of microplastic deformation and merging of clusters of deformation relief. The maximum value of the damage parameter D before the formation of a crack depends on a number of factors, however, in these studies does not exceed 0.8. The absence of signs of microplastic deformation in a certain number of crystallites is due to their unfavorable crystallographic orientation.

Stages of evolution of the fractal dimension Dp / s correspond to the peculiarities of the process of changing the damage parameter D. In addition, the

transition from intense change of the fractal dimension Dp / s to slowing down the process is accompanied by a merger of clusters.

The image of the deformation relief in the windows of the program for automated determination of fractal differences by the method of "box-counting" illustrates the phasing of surface defective structures. In Figure Figure 3.26 presents the image of the selected clusters at the stage of intensive growth of their number (Figure 3.16, a) and at the stage of saturation (Figure 3.16, b).

a) b)

Figure 3.14 - Clusters of deformation relief: a) N = 47300 cycles - the first stage;

b) N = 711000 cycles - the second stage. σ_{max}=173,15 MPa.

In Figure 3.19 present the evolution of quantitative parameters of the deformation relief D and Dp / s under load with maximum stress σ_{max}=173,15 MPa from zero cycle of tension (test series 2) and compression (series 3).

According to the obtained data, the difference between the current values of the studied parameters does not exceed 7.3%.

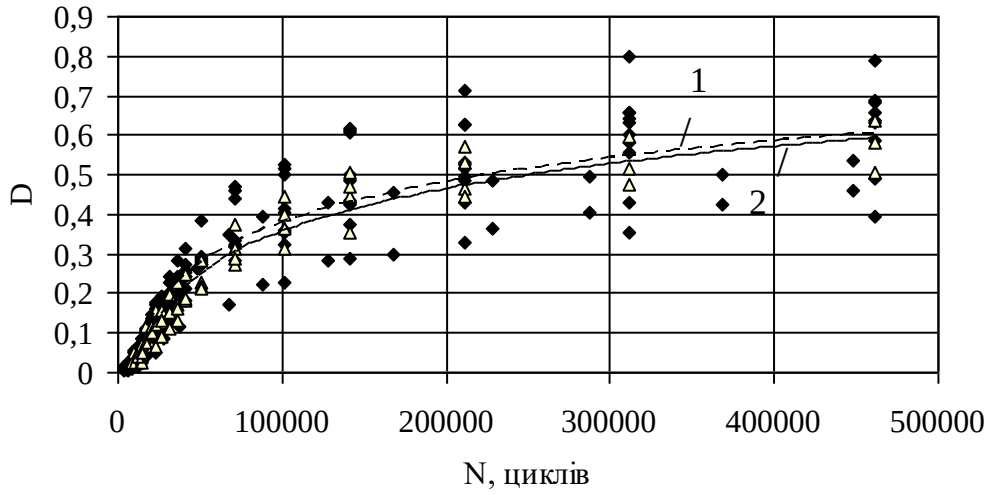

Figure 3.15 - Evolution of damage parameter D at tensile (1) and compressive (2) stresses, σ_{max}=173,15 MPa, series 2-3.

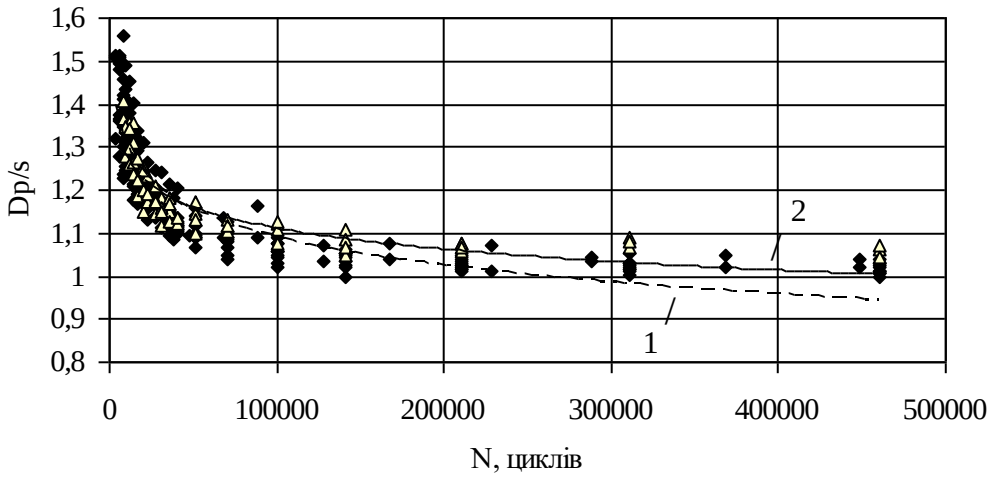

Figure 3.16 - Evolution of fractal dimension Dp / s at tensile (1) and compressive (2) stresses, σ_{max}=173,2 MPa, series 2-3.

With σ_{max}=173,2 MPa, R = 0 tested a series of samples (4 series), where the parameters were monitored both for the side where the tensile stress was applied and for the side where the compressive stress was applied (Figure 3.21-3.22). Polishing the samples on both sides significantly increased their durability.

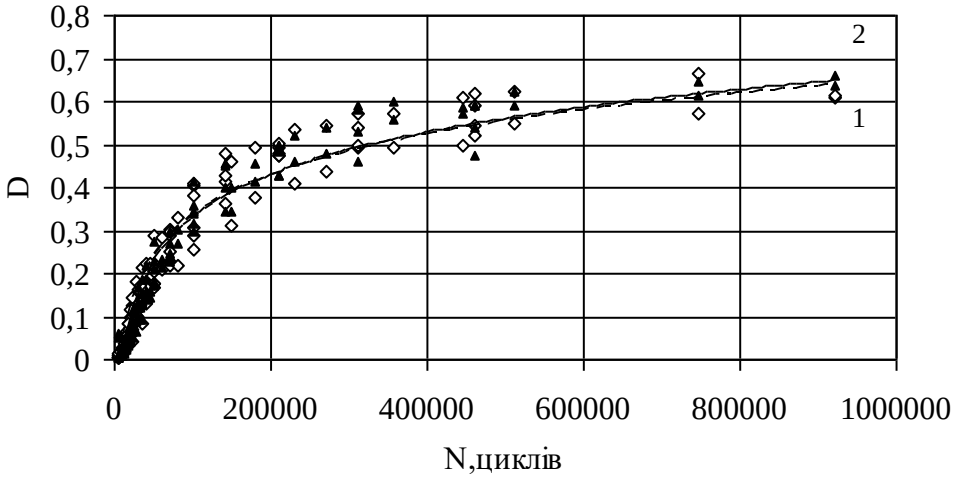

Figure 3.17 - Evolution of damage parameter D at tensile (1) and compressive (2) stresses, σ_{max}=173,2 MPa, series 4.

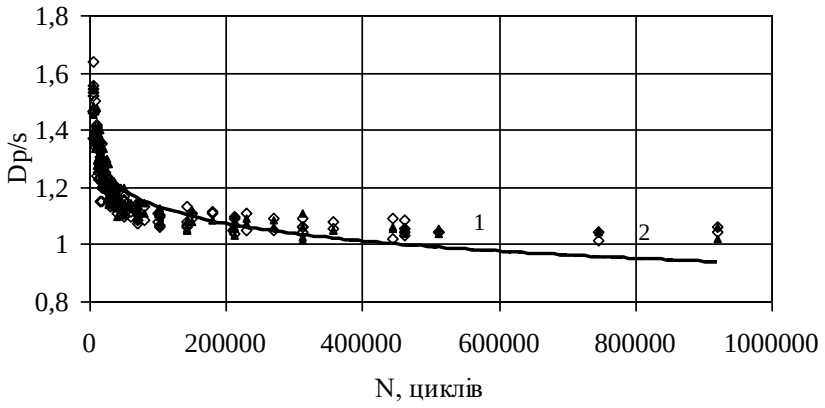

Figure 3.18 - Evolution of fractal dimension Dp / s at tensile (1) and compressive (1) stresses, σ_{max}=173,2 MPa, series 4.

3.3 Influence of the level of maximum stress of the load cycle on the development of deformation relief.

The influence of the level of the maximum stress of the loading cycle on the development of the deformation relief was investigated by testing compact samples at

zero load cycle with the maximum stresses of the cycle: 147.0 MPa; 173.2 MPa; 234.5 MPa (Table 3.5). The plastic zone near the stress concentrator in the form of a hole d = 1 mm on the side where the tensile stress acted was investigated. All samples were tested for destruction. The number of control points means the number of diametrically opposed plastic zones with a size of 0.3 mm at a distance of 0.02 mm.

Table 3.5 shows the data on the load modes and durability of the tested samples.

Table 3.5 - Modes of loading and durability of samples of series 1, 4 and 7.

№ series	№ sample	σ_{max}, MPA	Number of control points	N_{destr}, cycles
7	64	234,5	2	294800
	66	234,5	2	325700
4	56	173,2	2	1247100
	57	173,2	2	1497300
	58	173,2	2	985800
1	17	147,0	2	1584900

The results of monitoring the damage parameter D and the fractal dimension of the relief clusters, determined in relation to the perimeter of the clusters to their area Dp / s are shown in Figures 3.23- 3.24.

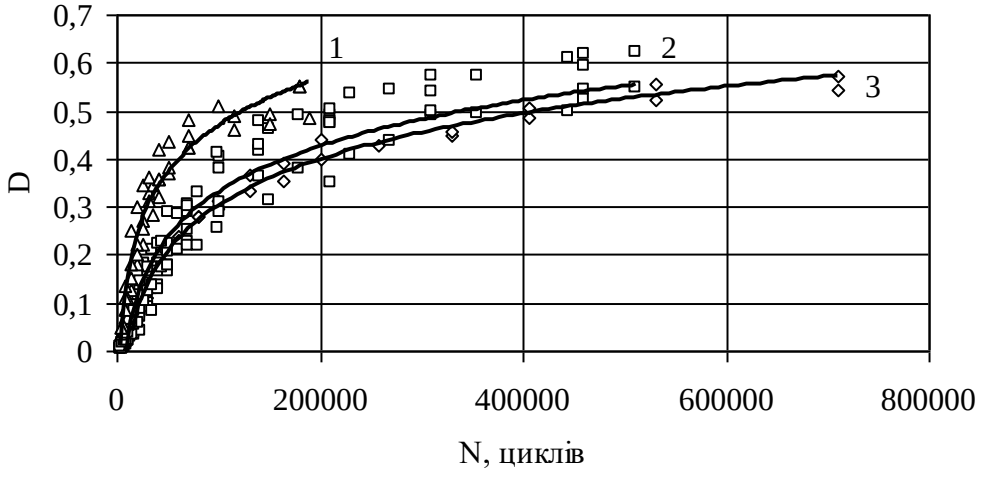

Figure 3.19 - Evolution of the damage parameter under cyclic loading, R = 0: 1) σ_{max}= 234,5 MPa; 2) σ_{max}= 173,2 MPa; 3) σ_{max}= 147,0 MPa.

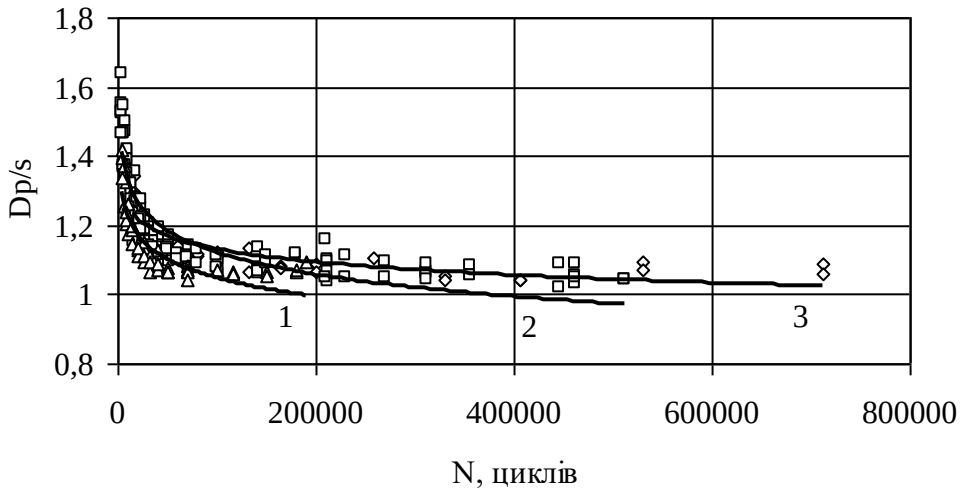

Figure 3.20 - Evolution of the fractal dimension Dps at cyclic loading, at R = 0:

1) σ_{max}= 234,5 MPa; 2) σ_{max}= 173,2 MPa; 3) σ_{max}= 147,0 MPa.

The tasks of forecasting the residual resource are best met by dependencies that allow you to estimate the current number of load cycles as a share of resource production, N_{cur}%, which is determined from the equation:

$$N_{cur}, \% = \frac{N}{N_{destr}} \cdot 100\% \quad .$$

(3.1)

In Figure 3.25 - 3.26 show the corresponding dependences.

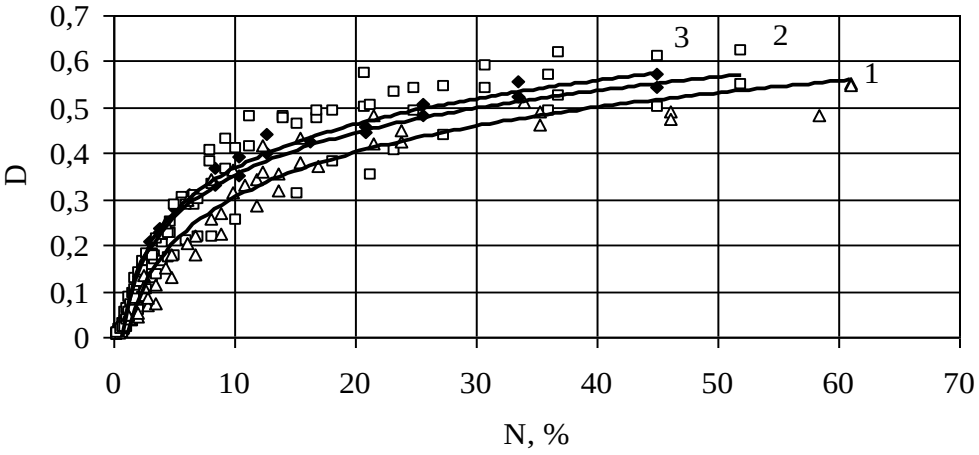

Figure 3.21 - Evolution of the damage parameter under cyclic loading in relative coordinates, R = 0: 1) σ_{max}= 234,5 MPa; 2) σ_{max}= 173,2 MPa; 3) σ_{max}= 147 MPa.

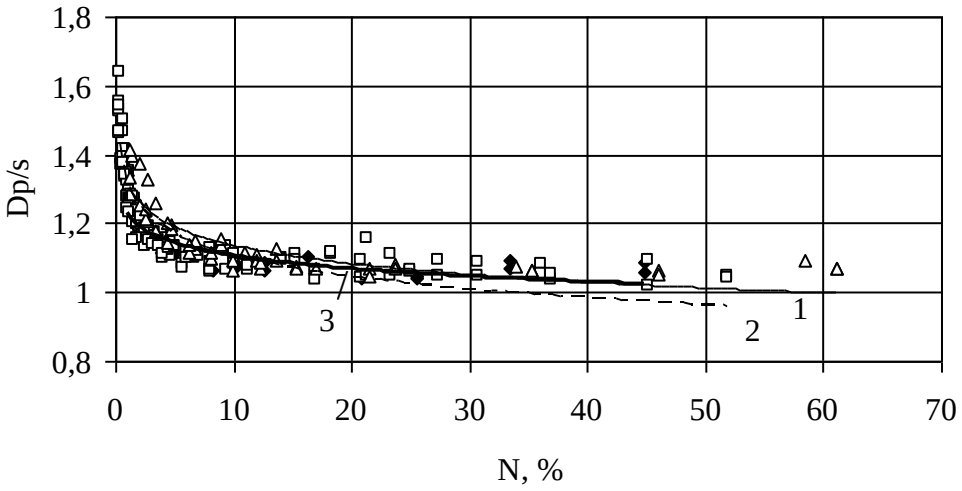

Figure 3.22 - Evolution of the fractal dimension Dps at cyclic loading in relative coordinates, R = 0: 1) σ_{max}= 234,5 MPa; 2) σ_{max}= 173,2 MPa; 3) σ_{max}= 147,0 MPa.

As can be seen from the graphs, the basic regularities of the dependences of the parameters of the deformation relief on the cyclic operating time for all the considered

modes of cyclic loading are of the same type. The most acceptable approximation equations (Table 3.6) of experimental data are logarithmic functions.

Table 3.6 - Equations of approximating curves of evolution of parameters deformation relief at different loading modes

Tension, MPa	Equation of approximating lines	Coefficient of determination, R^2
234,5	D = 0,1417 LnN – 1,1619	0,94
	$D = 0,1416\ LnN_{cur,\%} - 0,0234$	0,93
	Dp/s = - 0,0774 LnN + 1,9394	0,75
	$Dp/s = - 0,0774\ LnN_{cur,\%} + 1,3169$	0,74

End of the Table 3.6

173,2	D = 0,1375 LnN – 1,2525	0,92
	$D = 0,1332\ LnN_{cur,\%} + 0,0441$	0,91
	Dp/s = - 0,0914 LnN + 2,173	0,78
	$Dp/s = - 0,0899\ LnN_{пот,\%} + 1,3126$	0,79
147,0	D = 0,138 LnN – 1,287	0,98
	$D = 0,1381\ LnN_{cur,\%} + 0,0483$	0,99
	Dp/s = - 0,0544 LnN + 1,7572	0,72
	$Dp/s = - 0,0544\ LnN_{cur,\%} + 1,2314$	0,72

The obtained graphs also indicate the stage of the process of development of the deformation relief. The stage of intensive change of deformation relief parameters (1st stage) is approximately 20% of the total number of cycles before reaching the critical state. For samples tested under cyclic conditions.

The obtained graphs also indicate the stage of the process of development of the deformation relief. The stage of intensive change of deformation relief parameters (1st stage) is approximately 20% of the total number of cycles before reaching the critical state. For samples tested under cyclic tensile conditions, the critical state is a crack 1.0 mm long, for compact samples - their complete destruction.

Conclusion of the Part 3

The study of deformation relief at the micro level, in particular, the study of its dislocation structure by electron microscopy, as well as at the meso- and macro levels using optical microscopy using fractal image analysis, according to the developed method proved the fractal nature of deformation relief. This determined the possibility and expediency of using fractal geometry methods in monitoring the fatigue damage of the structural aluminum alloy D16AT.

Fatigue tests of D16AT alloy samples have shown that among the known fractal dimensions that can be used to describe clusters of deformation relief, the use of fractal dimension Dp / s, which is determined relative to the perimeter of the clusters to their area, is most appropriate. The dimension Dp / s is a characteristic of the shape of clusters of deformation relief and allows to significantly increase the accuracy of forecasting the residual life of structural elements when used in multiple

models together with the previously proposed damage parameter D, which determines the surface saturation with traces of microplastic deformation.

The process of formation and evolution of deformation relief is staged. In the first stage, the number of clusters of deformation relief and their total area increases, in the second stage, the slowdown in the growth of the total area of clusters coincides with their saturation.

4 LABOUR PROTECTION

4.1 Analysis of harmful and dangerous production factors

Two workplaces are used when carrying out all the needed procedures of the experiment. The first one is mechanical laboratory, used for the pure test conduction of the duralumin specimens. And the second one is open space personal computer workplace, where the CAE simulation is performed. In this chapter stress engineer working in front of a computer is considered as the subject of the work. Consequently, the office room layout working conditions will be analyzed.

4.1.1 Working conditions analysis

The workplace of a stress engineer is located in the office, which is the part of the engineering design center. There are two opposite each other workplaces in the room. They are quite similar and have one laptop on one side and personal computer on the other.

Geometrical sizes of the room are 3 m x 4 m x 3 m (length x width x height). Therefore, room area is 12 m2 and airspace is 36 m3. All these building parameters are approved by the state construction rules of Ukraine (ДБН В.2.2–28–2006) [15]. The size of the office room must be proportional to the number of engineers sitting in it. There is a plenty of room layouts, but fundamental principles for all of them are the same. It can be an open space zone, where the engineers' workplaces are separated with partitions and it can be an enclosed room, usually called as office unit.

Office room layout may be observed in the figure 4.1.

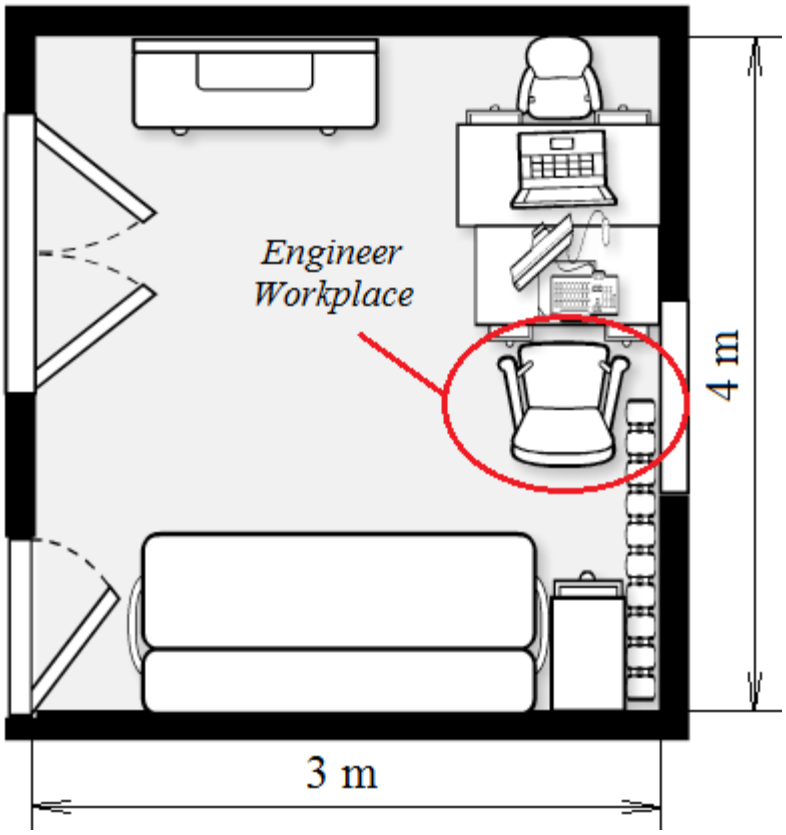

Figure 4.1 – Engineer room layout

Mixed lighting is used inside the room. Walls are mostly painted in the green, with some white inserts. There are two windows with metal frames and mechanical systems. The workplace itself (Figure 4.1) consists of the chair and the table. Leap chair featuring a 3D knit material on the back for aesthetic interest as well as added comfort, changes shape to mimic the movement of the spine and supports the body move. Table surface has the following dimensions: length 1680 mm, width 850 mm and height 700 mm. Natural Glide System technology allows to comfortably recline while keeping body aligned with the work so as not to strain eyes, neck, or arms. Also it has 4-way adjustable arms move in width, height, pivot to better support the neck

and shoulders and depth [16]. There are no galvanic or slip surfaces around the workplace.

The workplace in more details is shown in figure 4.2, according to the Order of the State Committee of Ukraine for Industrial Safety “On Approval of the Rules of Occupational Safety during Operation of Electronic Computing Machines” of 26.03.2010 No. 65 [17].

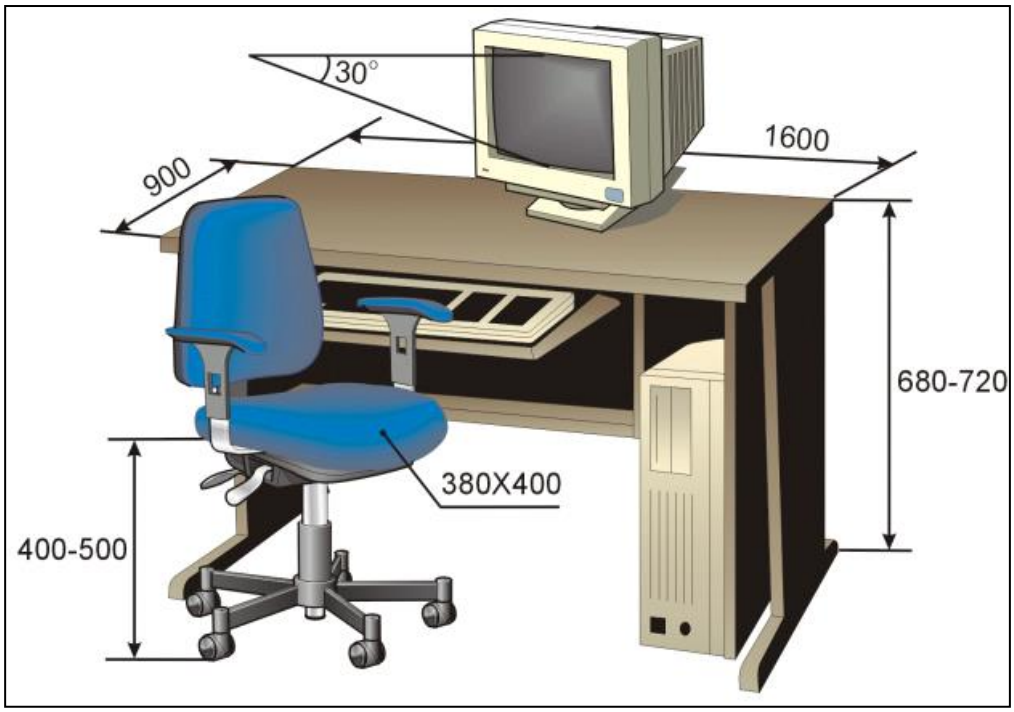

Figure 4.2 – Workplace layout [17]

Keyboard 160 mm from table edge. The distance between the monitor screen and the engineer's eyes is 650 mm. The monitor allows visual observation in a vertical plane at an angle of ± 20 ° from the working line. In winter, the indoor temperature is in the range of 19-23 ℃, and during warm periods - 23-26 ℃, and the relative humidity is usually around 40-60%. The air speed is 0.1 m / s. A fluorescent lighting system is used, as well as an air conditioning, heating and cooling system, optimal working conditions. Sources of noise are usually a personal computer (PC system

unit), a printer and an air conditioner. In case of fire, carbon dioxide fire extinguishers are placed. There is also a first aid kit, in addition to a special emergency department, which is located in the administrative building. More than 70% of the working time is spent by the engineer. However, there are special tables with electro-hydraulic drives that can be raised with a simple push of a button. They are designed in such a way that if the engineer is tired of sitting, he can raise the table and work in a standing position. It is very convenient and allows you to somehow warm up.

4.1.2 List of harmful and dangerous factors

1. Lack or absence of natural light;
2. Increased vibration level (local and general);
3. Increased level of ionizing radiation in the working area;
4. Increased noise in the workplace;

Since PC operation take the overwhelming majority of the working time, the sensory load takes place. But in this case it is not considered as a hazardous factor.

4.2 Measures to reduce the impact of harmful and dangerous production factors

Lamplight. Fluorescent lamps are used in this workroom. Two windows measuring 2 mx 1.5 m provide natural light. They have three-layer glass and a metal frame. Daylight factor ~ 1.6%. The actual light value is 210-255 lux. To provide artificial lighting in these areas, light sources with a sufficiently high efficiency should be placed in general lighting lamps, which are placed at workplaces in a uniform rectangular order. LED bulbs will be the best choice in these areas due to their maximum light output. Artificial lighting should provide illumination of the workplace with 300-500 lux. Artificial lighting significantly affects the vision of an engineer. The lack of lighting creates additional stress and, in the worst case, can even

lead to visual impairment. So, it is very important to take care of your eyes because they are the most loaded of all other parts of the body. Artificial lighting is used as a partial amount of natural light. Artificial lighting was used in these common areas. Only artificial light can be improved normally:

1. LB type fluorescent lamps are used as a source of artificial light;

2. Improving the lighting of the working space requires the reconstruction of the installed artificial lighting. One of these approaches can be the use of different types of lamps, changing their power and quantity. LED lamps were selected for installation. Unlike fluorescent lamps, LED lamps are capable of directly converting electrical current into light and, in theory, without large energy losses. LEDs do not heat up well and emit a narrow spectrum, and UV and IR radiation is usually absent. LEDs are mechanically robust and extremely reliable. The service life can reach 100 thousand hours, which is almost 5-10 times longer than that of fluorescent lamps. Finally, LEDs are low voltage devices, so they are relatively safe. The system switches are used to adjust the artificial light intensity according to the natural light intensity and your needs.

To ensure optimal performance and maintain the health of the engineer, regular breaks should be identified and established during shift. Timed breaks during a work shift should be established depending on the duration, type of work and category of employment. Continuous work without interruption should not exceed 2 hours.

With an 8-hour shift and work on a PC, a regulated break should be set: for work of category I - 2 hours from the beginning of the shift and every 2 hours after a lunch break of 15 minutes. Some eye exercises can be done to predict eye fatigue.

Microclimate: temperature, humidity, air speed. According to the required standards of ДСН 3.3.6.042-2006 “Санітарні норми мікроклімату виробничих приміщень”. Depending on the complexity of the work, the design engineers classified it as IB (light physical work). Optimal values of temperature, relative

Season	Category of works	Air temperature °C	Relative humidity, %	Speed, m/s
Cold	Easy – 1 b	21...23	40...60	0.1
Warm	Easy – 1 b	22...24	40...60	0.2

humidity and air velocity in the working area of commercial premises are shown in Table 4.1.

Table 4.1 – Optimal values of temperature, relative humidity and air speed

Table 4.2 – Permissible values of temperature, relative humidity and air speed

Season	Category of works	Air temperature, °C		Relative humidity, %	Speed, m/s
		Upper limit	Lower limit		
Cold	Easy – 1 b	24	20	75	not more 0.2
Warm	Easy – 1 b	28	22	60 at 27ºC	0.3–0.1

Table 4.3 – Actual values of temperature, relative humidity and air speed

Season	Category of works	Air temperature, C°	Relative humidity, %	Speed, m/s
Cold	Easy –1 b	18	35	0.25
Warm	Easy –1 b	20	30	0.35

To ensure an increase in humidity in a room with computer equipment, use humidifiers, which must be filled with distilled water daily. Reducing the negative impact of the microclimate is achieved through effective ventilation and heating. It is important to provide the office with a modern high-tech ventilation system. The point is that it can adjust the above parameters in two ways: automatically and manually. In addition, it has a control panel that allows you to change these parameters in each individual unit of the office space. Air filters should be installed in such a way as to prevent the entry of various biological hazards from the outside. Finally, a constant flow of air in an open space positively stimulates the human brain to work. Lack of fresh air can lead to serious health problems along with low productivity.

4.2.1 Working out the measures for labour protection improvement

To prevent or reduce the exposure of workers to harmful and dangerous production factors, collective and individual protective equipment is used. Collective protective equipment is designed to prevent, eliminate and reduce the impact of the following factors:

- vapors and dust of harmful substances, which leads to diseases of the respiratory system, disorders of the nervous system, dizziness, disorientation, loss of consciousness. The effect of the factor is eliminated by the normalization of the air environment in industrial premises and workplaces (ventilation, air conditioning, heating, automatic control and alarm);
- Excessive or insufficient lighting, leading to visual impairment and injury. It is eliminated by normalizing the illumination of industrial premises and workplaces (light sources, lighting equipment, light protective equipment, light filters);
- electric shock that can lead to death. Eliminated by the introduction of different types of enclosures, protective grounding, automatic shutdown, remote control;

- high temperatures of the equipment, leading to burns, provoking respiratory diseases, overheating, hypothermia. Eliminated by temperature control using ventilation, installation of heaters or air conditioners, enclosures, automatic control and alarm, thermal insulation, remote control.

4.2.2 Fire safety

Ensuring fire safety on the territory of Ukraine, the regulation of relations in this area by state bodies, local authorities, business entities and citizens should be carried out in accordance with “Кодекс цивільного захисту”, laws and other normative–legal acts.

- Room category

The room contains non-combustible substances and materials in the cold, therefore it corresponds to the category for explosion and fire hazard - "E".

- Type and number of fire extinguishers.

The main means of extinguishing a fire are carried out by a set of 2 dry powder fire extinguishers with 9 kg of agent.

- Sensor and fire alarm.

A fire alarm system has a number of devices working together to detect and alert people using visual and audible devices in the event of smoke, fire, carbon monoxide or other emergencies. These alarms can be triggered automatically by smoke and heat detectors, and can also be triggered by manual fire alarm activators such as manual call points or exhaust stations. Alarms can be either motorized bells or wall mountable sounders or horns.

Fire safety equipment is carried out in accordance with НАПБ А.01.001–2004 rules of fire safety in Ukraine. СПД-3 is selected for fire alarm sensor point. The sensor is designed for tracking the smoke in the 20 square meter area, so 3 sensors are placed symmetrically on the ceiling.

- Exits

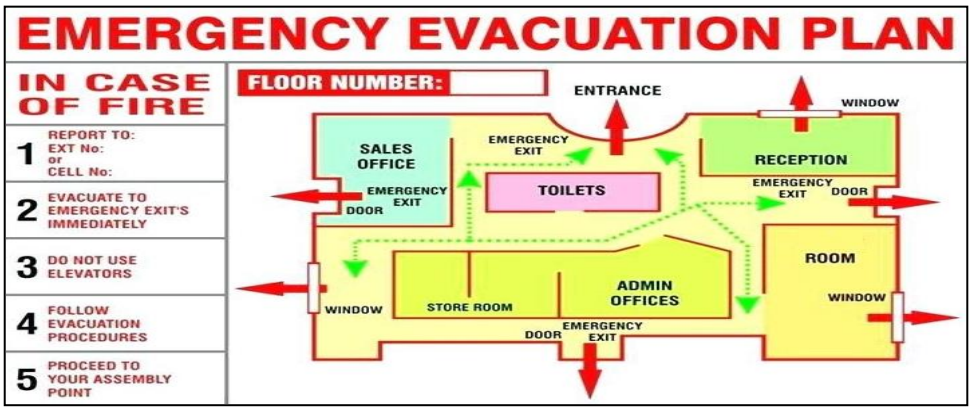

Figure 4.3 – Evacuation plan

Figure 4.3 shows clearly marked evacuation routes and emergency exits locations.

4.2.3 Artificial lighting calculation

Normal room illumination ($E_{\min}$) depends on the level of visual work performed in this room, which in turn is determined by the minimum size of the object of discrimination. For general lighting engineer at the lowest room illumination by ДБН В.2.5–28–2018 "Природне і штучне освітлення" [22] of at least 400 lx (lux). The actual value of light is 200 – 250 lx. Total light output is given by:

$$E_{gen} = \frac{E_n \cdot S \cdot k_1 \cdot k_2}{V} \quad (4.1)$$

where E_n – normalized illumination (E_n = 400 lx);

S – area of application;

– Coefficient taking into account the aging of lamps and lighting pollution (k_1 =1.2);

k k

– Coefficient taking into account the uneven illumination space (= 1.1);

V – Ratio of luminous flux, defined according to the reflection coefficient of walls, work surfaces, ceilings, room geometry and types of lamps.

Room size up: A = 3 m, B = 4 m, H = 3 m.

$$S = A \cdot B = 3 \cdot 4 = 12 \text{ m}^2 \quad (4.2)$$

Choose the table using the light flux ratios:

1. Reflection coefficient of whitewashed ceiling ($R_{ceiling}$ = 70%);
2. Index of refraction of white walls (R_{wall} = 55%);
3. Reflection coefficient from the dark hardwood floors (R_{floor}= 10%);
4. Index space ($i = (A \cdot B)/(h_{\downarrow}(p) \cdot (A + B))$.

$$h_p = H - h_n \quad (4.3)$$

where h_n– work surface height over the floor (h_n = 0.7 m).

Defining the room rate:

$$h_p = 3 - 0.7 = 2.3 \text{ m}$$

The utilization of light flux:

(4.4)

Now we define the value of the total luminous flux: (V=0.7)

$$E_{gen}\frac{400 \cdot 12 \cdot 1.2 \cdot 1.1}{0.7} = 9051\ lm \quad (4.5)$$

To ensure total artificial lighting, selected LED bulbs LED–T8SE–180 and replace fluorescent lamps 18W 990 lm. Luminous flux of one lamp LED-T8SE-180 (20W.). Thus, E_l=1650 lm.

Now we define the number of lamps required to illuminate the room:

$$N = \frac{E_{gen}}{E_l} = \frac{9051}{1650} = 6\ lamps \quad (4.6)$$

Thus, to provide light E_{gen} = 9051 lm output the 6 LED lamps must be used instead of 10 fluorescent lamps. Put in 2 rows. Power of 10 fluorescent lamps:

$$W_{gen}=W_N \cdot N = 18 \cdot 10 = 180\text{W} \quad (4.7)$$

Savings from the use of LED lamps.

$$N = W_{gen} / (N_{LED} \cdot P_{LED}) = 180/(6 \cdot 20) = 1.5 \quad (4.8)$$

Therefore, usage of LED lamps is more efficient.

4.3 Occupational Safety Instruction

4.3.1 General safety requirements

This Instruction provides the basic requirements for labor protection when working in a laboratory of electronic and microprocessor technology (hereinafter referred to as the laboratory). 1. When working in a laboratory, you must fulfill your duties in accordance with the requirements of this Instruction. 2. When working in a laboratory, students, a teacher (laboratory assistant) may be affected by the following hazardous and harmful production factors:

- a dangerous level of voltage in an electrical circuit, the closure of which can occur through the human body;
- live wires with damaged insulation;
- increased air temperature of the working area;
- increased temperature of equipment surfaces;
- increased level of electromagnetic radiation;
- increased level of static electricity;
- reduced air ionization;
- irrational organization of the workplace;
- insufficient illumination of the working area;
- increased tension of the organs of vision;
- static physical overload.

Sources of harmful and hazardous production factors:

- faulty equipment or improper operation;
- faulty electrical equipment or improper operation;
- absence, malfunction, improper use of PPE;
- absence, malfunction, improper operation of lighting devices;

- non-fulfillment or improper fulfillment of job descriptions, labor protection instructions, internal labor regulations, local regulations governing the procedure for organizing labor protection work, working conditions in the organization.

4.3.2 Safety Requirements before starting work

Check the availability and serviceability of personal protective equipment, if necessary, put on overalls that rely on the norms, put everything in order.

1. Fasten the overalls with all the buttons, avoiding hanging ends of the clothes. Do not pin clothes with pins, needles, do not keep sharp, fragile objects in pockets.

2. Check the serviceability of the PC, peripheral devices, technical teaching aids, other laboratory equipment, the integrity of the wire insulation.

3. Before starting work with measuring instruments, make sure that there are seals and a verification stamp.

4. Check the availability of software, install it if necessary.

5. Teaching aids, laboratory equipment, etc. can be conveniently placed on a demonstration table, as well as on students' tables (when conducting classes with students). The number of necessary equipment, components, wires to be placed at workplaces should be no more than one lesson.

6. Check the serviceability of the power supply network, compliance of its voltage with the voltage of the equipment used.

7. Prepare workplaces (yours and students) for safe work:

8. Inspect them, remove all unnecessary items without cluttering the passages.

9. Check approaches to workplaces, escape routes for compliance with labor protection requirements.

10. Check the presence and serviceability of safety devices, safety interlocks on the equipment.

11. Check the availability of fire protection equipment. A laboratory for extinguishing electrical equipment must be provided with carbon dioxide or powder fire extinguishers.

12. Check the availability and completeness of the first aid kit.

13. Establish a sequence of operations.

14. Check by visual inspection: - no hanging bare wires; - sufficiency of lighting of workplaces; - Reliability of closure of all current-carrying devices of the equipment; - the presence and reliability of grounding connections (absence of breaks, strength of contact between metal non-current-carrying parts of the equipment and the grounding wire); - absence of foreign objects around the equipment; - condition of floors (no potholes, irregularities, puddles, etc.); - the condition of the furniture (tables, chairs, shelves, cabinets).

15. Inform your immediate supervisor about all detected faults and malfunctions and start work only after they have been eliminated.

16. When conducting classes, laboratory work with students, make sure that they put on overalls, PPE (if necessary, use them) and take their places.

17. Conduct the following types of briefings:

- introductory (in the first lesson). Designed to familiarize students with the rules of conduct in the laboratory, the rules of occupational safety and health, fire safety, the dangerous moments that can be encountered in the process of work, and the appropriate precautions;

- primary at the workplace. Complements the introductory and aims to familiarize students with the organization and content of the workplace, equipment, with safe methods of working with it, with the rules for using personal protective equipment, with possible hazardous factors when performing a specific job, with the duties of a worker at his workplace, as well as with rules of conduct in the event of dangerous situations. The briefing should be accompanied by a demonstration of safe working techniques, followed by a check on the assimilation of knowledge;

- repeated. It is carried out once every six months under the program of initial instruction in the workplace;

- current. It is carried out before the start of specific laboratory or practical work.

In the process of work, in the event of a gross violation of labor safety requirements, which could result in injury to the offender or those working nearby, the teacher (laboratory assistant) is obliged to conduct an unscheduled briefing.

18. Record the conduct of briefings (except for the current one) in the class journal.

19. Proceed with work (conducting classes with students).

20. Work in the laboratory must be organized in accordance with the requirements of the current technological documents (norms, instructions, regulations), approved in the prescribed manner.

21. It is prohibited to start work (training) in the presence of the following violations of labor protection requirements

- in the presence of a malfunction specified in the operating manual of the manufacturer of laboratory and other equipment, in which its use is not allowed;

- in the absence or malfunction of personal protective equipment (if necessary, their use);

- in the absence of fire-fighting equipment, first aid kit;

- with insufficient illumination of the workplace and approaches to it;

- without instructing students on labor protection.

4.3.3 Safety Requirements during operation

1. Perform only the work for which you have been trained, instructed in labor protection and to which the employee responsible for the safe performance of work is admitted.

2. Do not allow untrained and unauthorized persons to work.

3. Apply proper laboratory equipment and technical training aids necessary for safe work; use them only for the work for which they are intended.

4. Monitor the operation of the equipment, periodically conduct its visual inspection in order to identify damage to its elements.

5. In case of detection of faulty equipment, other violations of labor protection requirements that cannot be eliminated on our own, and a threat to health, personal or collective safety, the teacher (laboratory assistant) should inform the management about this. Do not start work until the identified violations are eliminated.

6. When operating laboratory equipment, electrical equipment, teaching aids, etc., observe the rules for their operation in accordance with the instructions for labor protection.

7. Stop work using electrical equipment when:

- the appearance of extraneous noise, burning smell, power outage;
- absence or malfunction of protective grounding;
- fuzzy operation of the switch;
- malfunctions of safety, interlocking devices, other protective equipment;
- damage to the plug connection, wire insulation;
- with open live parts;
- the appearance of a noticeable electric current on the equipment body;
- breakage or cracks in the instrument case.

8. Assembly, installation of circuits, switching in them to carry out only in the absence of voltage.

9. Connect the wires without crossing them, pulling them or twisting them in loops.

10. The circuits collected by the students must be connected to the mains only after checking by the teacher (laboratory assistant) and with his permission.

11. When working with a PC:

12. Make sure that the screen is 5 degrees below eye level, and is located in a straight plane or tilted towards the worker (15 degrees).

13. Maintain the distance from the eyes to the screen within 60-80 cm.

14. Adjust visual parameters (image brightness and contrast) from minimum to maximum values using special knobs on the monitor case.

15. Place the local light source in relation to the workplace in such a way as to exclude direct light from entering the eyes and to ensure uniform illumination on a 40x40 cm surface, without creating blinding glare on the keyboard and monitor screen.

16. Periodically clean the monitor screen from dust.

17. To reduce visual and general fatigue, after each hour of work, take rest breaks of at least 5 minutes.

18. When working in the laboratory, it is prohibited:

- during classes, leave students unattended;

- to involve students in the performance of the duties of a laboratory assistant, to admit them to a laboratory assistant;

- to carry out work not provided for in the curriculum;

- to install circuits, switch connectors of interface cables of peripheral devices when the power is on;

- use the equipment improperly;

- use homemade devices;

- to allow the clutter of the workplace;

- turn off the power supply during the execution of an active task;

- to allow ingress of moisture on the surface and inside the equipment under voltage;

- leave the equipment turned on after the work has been completed;

- to carry out work without using the necessary PPE (if necessary, using them);

- work under the influence of alcohol, drugs, medications.

4.3.4 Safety Requirements after work

1. Disconnect electrical equipment from the mains.

2. Finish the lesson, dismiss the students.

3. Dismantle the laboratory equipment, put it in specially designated places in the laboratory.

4. Inspect and put in order the workplaces (yours and students).

5. Ventilate the room.

6. Take off your overalls. Contaminated overalls must be washed.

7. Wash hands thoroughly with soap.

8. Report to the management about all violations of the production process, labor protection requirements, cases of injuries at work.

4.3.5 Safety Requirements at emergency situations

1. In case of breakdown of laboratory equipment, other situation threatening an accident at the workplace:

- stop work;

- disconnect the equipment from the network;

- evacuate students to a safe place;

- report on the measures taken to the immediate supervisor (the person responsible for the safe operation of the equipment).

- act in accordance with the emergency response plan.

2. When a fire source appears, you must:

- stop work;

- disconnect the equipment from the network;

- evacuate students to a safe place;

- start extinguishing the fire immediately.

When electrical equipment catches fire, use only carbon dioxide or dry powder fire extinguishers.

3. If it is impossible to carry out extinguishing on their own, the teacher (laboratory assistant) should, in the prescribed manner, call the fire brigade and inform the immediate supervisor about it.

4. In case of injury or deterioration of health, stop working, inform the management and contact the first-aid post (call a city ambulance).

5. If an accident has occurred, witnessed by the teacher (laboratory assistant), he should:

- stop working;

- immediately report the incident to the immediate supervisor;

- Immediately withdraw or remove the victim from the danger zone;

- provide the victim with first aid;

- call a doctor or city ambulance;

- to help organize the delivery of the victim to the nearest medical facility.

6. In case of electric shock:

- stop the impact of electric current on the victim. This can be achieved by disconnecting the current source, breaking the supply wires, a switch, or by diverting the source of exposure from the victim. This should be done with a dry rope, stick, etc.

Do not touch the victim who is under the influence of the current with your hands.

- call a doctor or city ambulance;

- examine the victim. External damage must be treated and covered with a bandage;

- if there is no pulse, perform an indirect heart massage and artificial respiration.

It is necessary to carry out measures before the restoration of body functions or the appearance of signs of death.

7. When investigating the circumstances and causes of the accident, the teacher (laboratory assistant) should inform the commission about the information he knows about the accident.

Conclusion to Part 4

Labour protection is a very important part of any engineering process, as it decreases risks of fatal events and increases human survivability in emergency situations. Therefore, any workplace should meet the requirements concerning labour and life safety. In this part the working place in front of a computer was represented in details. Geometrical characteristics of the office room were calculated. The most hazardous factors during operation in work were listed and made propositions for improvement of these conditions. There was represented evacuation plan in case of fire event and artificial lighting improvement has been proposed and proved by calculations.

Everything meets the Labour Protection requirements and standards of Ukraine.

5 ENVIRONMENTAL PROTECTION

5.1 Introduction

The environmental impact of aviation occurs because aircraft engines generate heat, noise, particles and gases that contribute to climate change and global dimming. Airplanes emit particles and gases such as carbon dioxide (CO2), water vapor, hydrocarbons, carbon monoxide, nitrogen oxides, sulfur oxides, lead and black carbon that interact with each other and with the atmosphere. Despite declining emissions from cars and more fuel efficient and less polluting turbofans and turboprop engines, the rapid growth in air travel in recent years has contributed to an increase in overall aviation-related pollution. From 1992 to 2005, passenger traffic increased by 5.2% per year. And in the European Union, greenhouse gas emissions from aviation increased by 87% between 1990 and 2006. A comprehensive study shows that despite expected innovations in efficiency for airframe, engines, aerodynamics and flight, there is no end, even many decades, for the rapid rise in CO2 emissions from air travel and air travel due to the projected constant growth in air travel. This is because international aviation emissions escaped international regulation up until the three-year ICAO conference in October 2016, aligned with the CORSIA offset system, and with no taxes on aviation fuel around the world, lower tariffs are becoming more frequent than otherwise. case, which gives a competitive advantage over other modes of transport. If market caps are not put in place, this increase in aviation emissions would result in sector emissions accounting for all or nearly all of the annual global CO2 emissions budget by mid-century, if climate change is sustained until temperatures rise by 2°C, or less. Discussions are ongoing about the possible taxation of air travel and the inclusion of aviation in the emissions trading scheme to ensure that the overall external costs of aviation are taken into account.

5.2 Environmental pollution classification

5.2.1 Acoustic pollution

Airborne noise manifests itself in propaganda groups as very difficult to get attention and take action. The main challenges are increased traffic at major airports and airport expansion at smaller and regional airports. Aviation authorities and airlines have developed continuous descent procedures to reduce noise. The current current noise

standards in effect since 2014 are FAA Stage 4 and (equivalent) EASA. Chapter 4. Aircraft with lower standards are limited by a time window or, at many airports, are completely banned. Phase 5 will take effect between 2017 and 2020. Quantifying and comparing noise effects per seat spacing takes into account that noise from cruise levels usually does not reach the earth's surface (unlike ground vehicles), but is concentrated in and around airports.

The admissible noise levels and the method of their measurement for aircraft of various categories are formulated (the year of manufacture, the number of engines and their type, values of the maximum certified take-off weight of the aircraft are taken into account).

For the development of noise reduction technologies, the Independent Group created by CAEP (Committee on Aviation Environmental Protection), experts formulated medium-term (until 2020) and long-term (until 2030) technological goals. They are standards that will be mandatory for four categories of aircraft in 2030 (Table 5.1). Targets are shown as noise abatement values relative to nominal and maximum take-off weights [27]. The noise level is measured in units of EPNdb - effectively perceived noise level in decibels. Considering that in 2014 [26] these levels, depending on the type of aircraft, were 89-106 EPNdb, it becomes obvious how radically ICAO is going to combat acoustic pollution of the atmosphere.

Table 5.1 - Estimated long-term prospects for aircraft noise reduction by 2030

Aircraft category	Long term goals, EPNdb
Regional jet aircraft	
40 t (nominal)	21.5 ± 4
50 t (maximum)	17 ± 4
Twin-engine short / medium range aircraft	
Turbofan:	
78 t (nominal)	30 ± 4
98 t (maximum)	26.5 ± 4
With bi-turbo fan engines	
78 t (nominal)	13.5 + 2 / -6
98 t (maximum)	10.5 + 2 / -6
Twin-engine trunk aircraft	
230 t (nominal)	28 ± 4
290 t (maximum)	24.5 ± 4
Four-engine trunk aircraft	
440 t (nominal)	27 ± 4
550 t (maximum)	20.5 ± 4

5.2.2 Water pollution

Airports can generate significant water pollution due to their widespread use and handling of jet fuel, lubricants and other chemicals. Airports establish spill control structures and related equipment (eg vacuum trucks, portable berms, absorbents) to prevent chemical spills and mitigate the consequences of spills that do occur.
In cold climates, the use of de-icing fluids can also cause water contamination, as most fluids applied to aircraft subsequently fall to the ground and can be transported through storm runoff into nearby rivers, rivers, or coastal waters.: 101 Airlines use ethylene glycol-based de-icing fluids or propylene glycol as an active ingredient. Ethylene glycol and propylene glycol are known to exhibit high levels of biochemical

oxygen demand (BOD) during degradation in surface waters. This process can adversely affect aquatic life by consuming oxygen that aquatic organisms need to survive. Large amounts of dissolved oxygen (DO) in the water column are consumed when microbial populations degrade propylene glycol. Adequate levels of dissolved oxygen in surface waters are critical for the survival of fish, macroinvertebrates, and other aquatic organisms. If the oxygen concentration falls below the minimum level, organisms emigrate, if possible and possible, to areas with higher oxygen levels, or eventually die. This effect can significantly reduce the number of usable aquatic life. Reducing DO levels can reduce or eliminate bottom food populations, create conditions conducive to changing the species profile of a community, or alter critical interactions with food on the Internet. -2-30.

5.2.3 Air quality. Particulate matter emissions

Ultrafine Particles (UFP) are emitted from aircraft engines during near-surface operations, including taxis, takeoff, ascent, descent and landing, and idling at gates and taxiways. Other sources of UFP include ground support equipment operating around terminal areas. In 2014, an air quality study found that the area exposed to ultrafine particles from takeoffs and landings on a leeward flight at Los Angeles International Airport is much larger than previously thought. Typical UFP emissions during take-off are in the order of 1015-1017 particles emitted per kilogram of fuel burned. Emissions of non-volatile soot particles are 1014-1016 particles per kilogram of fuel on a quantity basis and 0.1-1 g per kilogram of fuel on a mass basis, depending on engine and fuel characteristics.

Chemical pollution of air at airports is represented by such aviation emissions as oxides of carbon (CO, CO_2), nitrogen (NO_x), sulfur (SO_x), hydrocarbons (HC) and suspended particles resulting from the operation of engines and combustion of aviation fuel (Figure 5.1).

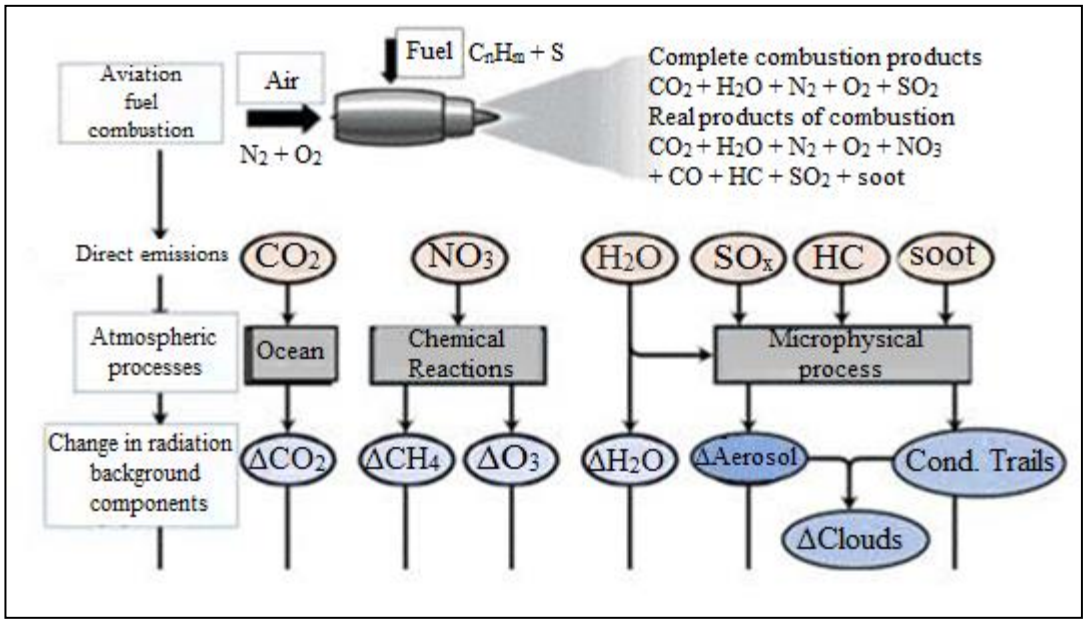

Figure 5.1 – The impact of aviation emissions on the environment

Aviation-related emission sources can spread and degrade air quality in nearby communities. These emissions pose a potential risk to public health and the environment as they can increase ground-level ozone and lead to acid rain. National and international air quality monitoring programs routinely require authorized aviation and government agencies to monitor air quality near airports. Particular attention is also paid to the environmental impact of aviation related to water quality, waste disposal, energy consumption, as well as local environmental impacts in the vicinity of airports (prevention of fuel leaks is especially important).

5.2.4 Chemical pollution

About 167,000 piston-engine aircraft - about three-quarters of private aircraft in the United States - release lead (Pb) into the air from lead aviation fuel. From 1970 to 2007, the general aviation aviation released about 34,000 tons of lead into the atmosphere according to the Environmental Protection Agency. Lead is recognized as a serious environmental threat by the FAA if inhaled or swallowed, resulting in adverse effects on the nervous system, red blood cells, and the cardiovascular and immune systems in infants and young children, especially sensitive to even low levels of lead, which can contribute to behavioral and academic problems, IQ decline and autism.

The ICAO Engine Emission Bank (EEDB) contains information on the EI values for certified engines (in grams of pollutant per kilogram of fuel for NOx, CO and HC), as well as the consumption of special fuels (kilograms per second) for different operating modes of different types of engines. In addition, the smokiness number is indicated here - a dimensionless parameter calculated on a 10-point scale and characterizing smoke emission as the "opacity" of the exhaust stream. The emission figures for the PW4074D engine installed on the Airbus A330 are shown, for example, in Table 5.2.

Table 5.2 – Emission for the PW4074D engine of the ICAO emission data bank

Operating Mode	Engine Power, %	Time, min	Fuel Consumption, kg/s	Fuel Emission Index, g/kg			Smokiness Number
				HC	CO	NO_x	
Take-off	100	0.7	3.042	0.02	0.3	42.46	4.22
Climb	85	2.2	2.471	0.02	0.35	32.71	2.36
Descent	30	4.0	0.869	0.04	0.96	11.35	0.65
Idle	7	26.0	0.305	3.12	26.34	3.8	0.33
Fuel (kg) and emissions (g) for cycle			1138	1502	12885	20269	-

5.2.5 Radiation exposure

Flying 12 kilometers (39,000 feet) in altitude, passengers and crews of jet liners are exposed to at least 10 times the dose of cosmic rays that humans receive at sea level. Every few years, a geomagnetic storm allows a solar particle event to penetrate down to the heights of a jet plane. Aerial flying polar routes near the geomagnetic poles are at particular risk.

5.2.6 Changing of the climate

Like all human activities associated with combustion, most forms of aviation release carbon dioxide (CO2) and other greenhouse gases into the Earth's atmosphere, which

contribute to accelerating global warming and (in the case of CO2) ocean acidification. This concern is underlined by the current volume and growth of commercial aviation. Worldwide, about 8.3 million people fly daily (3 billion occupied seats per year), which is double the 1999 level. US Airlines alone burned about 16.2 billion gallons of fuel in the twelve months from October 2013 to September 2014.

In addition to the CO2 emitted by most aircraft in flight by burning fuels such as Jet-A (turbine aircraft) or Avgas (piston aircraft), the aviation industry also contributes to greenhouse gas emissions from airport ground vehicles and those used by passengers and staff. for access to airports; and emissions from energy production for airport buildings, aircraft manufacturing and airport infrastructure construction.

While the main greenhouse gas emissions from operating aircraft in flight are CO2, other emissions can include nitrogen oxide and nitrogen dioxide (collectively called nitrogen oxides or NOx), water vapor and particles (soot and sulphate particles), sulfur oxides, oxide carbon (which binds to oxygen immediately after CO2 is released), hydrocarbons, tetraethyl elude (piston aircraft only) and radicals such as hydroxyl, depending on the type of aircraft used, are incompletely combusted. Emission Specific Gravity (EWF), ie. The factor at which aviation CO2 emissions must be multiplied to obtain CO2 emissions equivalent for the average annual fleet status is in the range 1.3-2.9.

5.2.7 Aircraft Engine Emissions

Aircraft engines produce emissions similar to those from burning fossil fuels. However, aircraft emissions are unusual in that a significant proportion of them are generated at altitude. These emissions pose serious environmental problems due to their global impact and impact on local air quality at ground level.

The bulk of aviation fuel burns not in the surface layer near airports, but in the higher layers of the atmosphere. Experts believe that the increasing annual emissions of carbon dioxide, water and methane from commercial aircraft engines alter the chemical and radiation balance of the atmosphere, which, along with the release of carbon black sulphate aerosols, can affect the climate (Figure 5.1). Components such as carbon dioxide and nitrogen oxides are of particular importance. Nitrogen oxides take part in the chemical composition of ozone (its increase can lead to heating of the

upper troposphere) and an increase in the amount of hydroxyl radicals (OH), the main oxidant of the atmosphere.

Among the combustion products of aviation fuel are greenhouse gases, emissions of which can contribute to global warming. To reduce these, airlines have only two options. First, it is an increase in fuel efficiency (ie, specific fuel consumption).

The second is the use of alternative fuels: synthetic fuels from coal, natural gas or biomass. Natural fuel does not contain sulfur and aromatic hydrocarbons, which significantly reduces emissions of volatile aerosols and cloud condensation nuclei, thereby weakening the impact on the radiation balance. In addition, model experiments have shown that the use of fuel, purified from sulfur, leads to a significant ecological "recovery" of the troposphere in terms of the concentrations of ozone, sulfates and nitrates (Figure 5.2.)

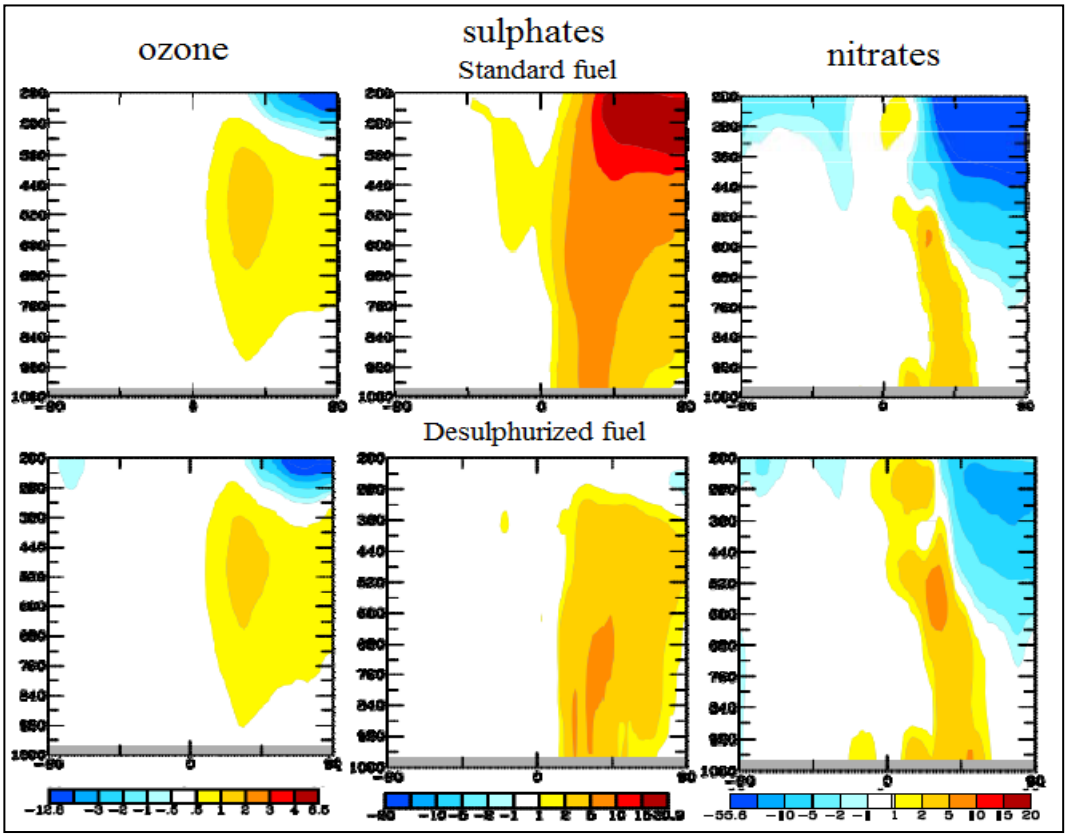

Figure 5.2 – The effect of aviation emissions on annual and mid-seasonal concentrations (in %) of ozone, sulfates and nitrates for standard and sulfur-purified fuel. The vertical axis is the pressure in GPa, the horizontal axis is latitude in degrees.

It should be noted that the attitude of specialists to biofuels (made from corn, soybeans, rapeseed, palm oil, algae, etc.) is far from unambiguous in conditions when crops often die due to droughts or untimely rains. Experts warn that a complete transition to biofuels threatens the gradual destruction of tropical forests and higher prices for food. In addition, the effect of reducing CO2 emissions has not been proven with long-term use. Nevertheless, biofuel for aviation needs is already being produced in the USA, Great Britain, Germany, France, Finland [40]. By 2020, China, which has launched production of fuel from palm oil, also intends to increase the share of biofuels to one third of all fuels used by aviation. In recent years, a number of ecology-friendly countries have been actively replacing traditional aviation kerosene with cryogenic fuel (hydrogen, liquefied natural gas). When used, the aircraft becomes more economical (fuel consumption is reduced), CO2 emissions into the atmosphere are reduced.

5.3 Multiaxial stress test environmental conditions

Instron 8874 axial-torsional testing stand has been used for experiment (Figure 5.3).

Figure 5.3 – Instron 8874 axial-torsional testing stand

Every care has been taken in the design, assembly and testing of this equipment.

However, it is impossible to completely isolate it from the effects of the environment in which it has been stored prior to installation and the operating environment.

To eliminate unnecessary downtime and maximize your testing performance equipment, it is important to pay particular attention to providing a high quality work environment, both physical and electrical.

Physical environmental conditions such as high ambient temperatures or excessive humidity may cause overheating or physical damage to internal components. Prolonged exposure to acid fumes, carbon black, or other conductive dust can cause electrical problems. Electrical noise can cause problems; loss or loss of data, unexplained errors, resets, or other malfunctions. AC power from a wall outlet is often a major source of problems. For many reasons, the normal power supply can be filled with surges, surges and other unwanted noise interference. Even if the original power line is okay, electrical noise can be caused on power lines by internal factory equipment, air conditioners, office appliances, and fluorescent lamps.

Instron 8800 series controllers have a noise level of <70 dBA. The noise level of the entire system depends on the specific system configuration. For information on the noise level of this component, refer to the documentation provided with each

component in your system. In terms of noise, the OSHA (Occupational Safety and Health Administration) PEL is 90 dBA for all workers during an 8-hour workday. The OSHA standard uses an exchange rate of 5 dBA. This means that when the noise level increases by 5 dBA, the time that a person can be exposed to a certain noise level to receive the same dose is halved. Thus, it is concluded that the machine meets the requirements of the standard. The test pieces were made of duralumin, which is an aluminum alloy. Aluminum is one of the most environmentally friendly metals. The high regenerative capacity of aluminum is one of the environmental advantages of this material.

It is easily recyclable and can be reused an unlimited number of times. Its production is much less harmful to the environment than the production of other metals. The use of recycled aluminum from scrap and waste recycling allows you to save up to 95% of the energy required for smelting primary metal, conserve natural resources and significantly reduce emissions of gases such as CO2, NO2, SO2. For example, emissions of pollutants from nickel production exceed those of the aluminum industry by 31 times, and specific emissions of sulfur dioxide are on average 387 times. Higher Consequently, multiaxial stress tests do not pose a threat to the environment. All conditions are in accordance with the relevant standards.

Conclusion to Part 5

Civil aviation takes measures to reduce the negative impact of aviation on the environment. To this end, new standards are being developed that tighten the requirements for aircraft operation in terms of aircraft noise and emissions, and the list of aircraft emissions for which aircraft engines are certified is being expanded. The ICAO Committee on Environmental Protection proposes a Global Market Action Mechanism as the primary instrument for managing the negative impact of aviation on the atmosphere. While this idea is not supported by all ICAO members, the need for new technologies in the aviation industry to reduce the environmental impact of air transport is clear.

Ukraine fully supports ICAO's environmental policies and practices as outlined in ICAO Assembly Resolution A39-2 and strives to achieve the global aspirational goal of carbon neutralization from international aviation from 2020, as well as implement a global market mechanism in 2020 designed to reduce emissions ... emissions from civil aviation. At the same time, the market mechanism should take into account the principle of joint but differentiated responsibility and corresponding opportunities, special circumstances, as well as the principle of non-discrimination and equal and fair opportunities.

With regard to environmental conditions during multiaxial stress tests, Instron 8874 and duralumin samples fully meet the requirements of the standard.

GENERAL CONCLUSIONS

The thesis consists of five main parts: theoretical information about the nature of multiaxial loading and its presence in the structural elements of the aircraft; materials, samples and experimental procedures; results of experiments, including testing on modeling by the finite element method in the Abaqus program, invention and proposal of a method for assessing fatigue damage to aircraft components; part of labor protection and part of environmental protection. The first part focuses on the type of aircraft loads, explains the nature of multiaxial stresses and explains why it is so important to take them into account. The second part is devoted to the experimental technique. Four fatigue tests were performed on the Instron 8874 machine. Specimens of D16AT aluminum alloy coated with pure aluminum foil (99.99% Al by mass) were tested in the following modes: pure tension-compression test, pure torsion, complex in-phase and complex external loading. With the help of optical and scanning microscopy, the images of the deformation surface of the relief were enlarged 250 and even 500 times. The Abaqus program made it possible to simulate the test using the finite element model created in Catia. It was necessary to observe the stress distribution on the surface of the test sample. In the third part, the results of the experiment are presented in a visual form, allowing to assess the patterns of damage accumulation and to propose a method for its assessment. The damage coefficient is proposed as a numerical characteristic of multiaxial fatigue damage. The antiphase mode turned out to be the most important, since it has the largest slope angle and derivative compared to the fracture curves for other modes. It has been proved that the density of slip bands (extrusions / penetrations) depends not only on the stress level and the number of

cycles, but also on the type of loading and the nature of its application. The fourth part is devoted to labor protection. It was considered a computer place to work according to the labor protection standards of Ukraine. The fifth part is devoted to the protection of the environment from various types of aviation pollution: water pollution, air pollution, acoustic, chemical and others.

REFERENCES

1. https://lingualeo.com/ru/jungle/g-longhurst-aeroplane-performance-2-430315.
2. Dept. of Aerospace Engg., Indian Institute of Technology, Madras Flight Dynamics Chapter-9.
3. CLICK2PPSC LTD EDITION 2.00.00 2001.
4. КОНСПЕКТ ЛЕКЦИЙ по дисциплине "Конструкция и прочность летательных аппаратов" Ч.2, профессор А.И. Радченко.
5. Ali Fatemi -University of Toledo Chapter 10 – Multiaxial Fatigue.
6. MSC. Fatigue User's Guide. www.mscsoftware.com.
7. Dr NWM Bishop, Sherrart F. Finite element based fatigue calculations. Published by NAFEMS Ltd, Whitworth
8. Building, Scottish Enterprise Technology Park, East Kilbride, Glasgow, G75 OQD, October 2000.
9. Dang Van, K., Cailletaud, G., Flavenot, J.F., Le Douaron, A., Lieurade, H.P. Criterion for High Cycle Fatigue Failure Under Multiaxial Loading, Biaxial and Multiaxial Fatigue. Mechanical Engineering Publications. 1989.
10. Стрижиус В.Е. Методы и процедуры расчетов на усталость элементов авиационных конструкций. - М.: Изд-во МАИ-ПРИНТ, 2008.

11. H. L. Cox and W. J. Clenshaw. The behaviour of three single crystals of aluminium in fatigue under complex stresses.

12. Ł. Pejkowski, M. Karuskevich, T. Maslak Extrusion/intrusion structure as a fatigue indicator for uniaxial and multiaxial loading. Fatigue Fract Eng Mater Struct. – 2019. - Volume 42. Issue 10 – P.2315-2324.

13. http://bitimpex-zs.com/aluminum-sheet-d16at-d16am-d16.html.

14. https://www.instron.us/en-us/products/testing-systems/dynamic-and-fatigue- systems/servohydraulic-fatigue/8874-axial-torsion.

15. http://kbu.org.ua/assets/app/documents/dbn2/73.1.pdf.

16. https://store.steelcase.com/seating/office-chairs/leap-3d-knit.

17. https://www.victorija.ua/dovidnik/osnovni-pravyla-dotrymannya-ohorony-pratsi- pry-roboti-na-personalnyh-eom.html.

18. https://zakon.rada.gov.ua/laws/show/z0472-14.

19. http://online.budstandart.com/ua/catalog/doc-page?id_doc=14283.

20. https://zakon.rada.gov.ua/laws/show/5403-17.

21. https://dnaop.com/html/31612/doc-90.01.001-2004.

22. http://www.gorsvet.kiev.ua/wp 2018 pdf.

23. https://en.wikipedia.org/wiki/Environmental_impact_of_aviation.

24. https://www.icao.int/environmental-protection/Pages/default.aspx.

25. Khaletsky Y.D. ICAO: A New Standard for the Noise of Civil Aviation Aircraft // Engines. 2014. No. 2 (92). Pp. 8-11.

26. Environmental protection. Volume 1. Aviation Noise: Annex 16 to the Convention on International Civil Aviation. ICAO, Issue 3, July 2008.

27. Civil Aviation Events and the Environment: Working Paper of the 38th Session of the ICAO Assembly - www.icao.int.

28. ICAO Aircraft engine emission Databank. November 2016. https://www.easa.europa.eu/documentlibrary/icao-aircraft-engine emissionsdatabank.

29. Guidance material on aviation emission charges related to local air quality. Doc. 9884. - ICAO, 1st edition, 2007.

30. Airport Air Quality Manual. Doc9889. ICAO, First edition, 2011.

31. Environmental protection. Volume 2. Emission of aircraft engines: Annex 16 to the Convention on International Civil Aviation. ICAO, Issue 5, July 2014.

32. Lee D., Fahey D.W., Forster P.M. et al. Aviation and global climate change in the 21st century // Atm. Environ. 2009. Vol. 43. P. 3520-3537.

33. Olsen S.C., Brasseur G.P., Wuebbles D.J., Barret S.R.H. et al. Comparison of model estimates of the effects of aviation emissions on atmospheric ozone and methane // Geophys. Really. Let. 2013. Vol. 40. P. 6004-6009. doi: 10.1002 / 2013GL057660.

34. On Board. A sustainable future. Environmental Report. - ICAO, 2016.

35. A.M. Starik, A.N. Favorsky. Aviation and atmospheric processes // Current problems of aviation and aerospace systems. 2015. Vol. 20, No. 1 (40). Pp. 1-20.

36. Popovicheva O.B., Starik A.M. Aviation soot aerosols: physicochemical properties and consequences of emission into the atmosphere // Izvestiya RAS. PAO. 2007. Vol. 43, No. 2. Pp. 147-164.

37. Popovicheva O.B., Persiantseva N.M., Zubareva N.A., Shonia N.K., Starik A.M., Savelyev A.M. Soot aerosols in the upper troposphere: properties and consequences of aviation emissions. SRINP MSU, 2005, 83 p.

38. Unger N. Global climate impact of civil aviation for standard and desulfurized jet fuel // Geoph. Really. Lett. 2011. Vol. 38. L20803. doi: 10.1029 / 2011GL049289.

39. Nikiforov O. Hunger as an alternative to biofuels. http://www.ng.ru/ng_energiya/2012 09-11 / 15_hunger.html.

40. https://www.aviaport.ru/news/2012/07/27/238185.html.

41. http://www.bioethanol.ru/bioethanol/news/kitajj_nachinaet_ispolzovat_biotoplivo_v_grazhdanskojj_aviatsii/.

42. V.A. Andreev, V. Solobozov, Fuel for 21st Century Aircraft // Science and Life. 2001 № 3. Pp. 23-25.

43. The EU Emission Trading System (EU ETS). - European Union, 2016.

44. http://www.greenaironline.com/news.php?viewStory=2021.

45. www.instron.com. Reference Manual - Configuration.

46. https://www.osha.gov/SLTC/noisehearingconservation/.

47. https://pandia.ru/text/77/277/66268.php.